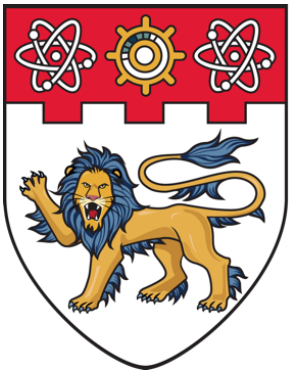

NANYANG TECHNOLOGICAL UNIVERSITY
SINGAPORE

VOLATILE-BASED DIAGNOSIS FOR PATHOGENIC WOOD ROT FUNGI AFFECTING SINGAPORE URBAN TREES

TAN JHING YEIN

SCHOOL OF BIOLOGICAL SCIENCES

2024

VOLATILE-BASED DIAGNOSIS FOR PATHOGENIC WOOD ROT FUNGI AFFECTING SINGAPORE URBAN TREES

TAN JHING YEIN

SCHOOL OF BIOLOGICAL SCIENCES

A thesis submitted to the Nanyang Technological University in partial fulfilment of the requirement for the degree of Master of Science

2024

Statement of Originality

I hereby certify that the work embodied in this thesis is the result of original research done by me except where otherwise stated in this thesis. The thesis work has not been submitted for a degree or professional qualification to any other university or institution. I declare that this thesis is written by myself and is free of plagiarism and of sufficient grammatical clarity to be examined. I confirm that the investigations were conducted in accord with the ethics policies and integrity standards of Nanyang Technological University and that the research data are presented honestly and without prejudice.

06/02/2024

. . . . . .

Date

. . . . . .

Tan Jhing Yein

Supervisor Declaration Statement

I have reviewed the content and presentation style of this thesis and declare it is free of plagiarism and of sufficient grammatical clarity to be examined. To the best of my knowledge, the research and writing are those of the candidate except as acknowledged in the Author Attribution Statement. I confirm that the investigations were conducted in accord with the ethics policies and integrity standards of Nanyang Technological University and that the research data are presented honestly and without prejudice.

06/02/2024

. . . . . .

Date

. . . . . .

Dr Hong Yan

Authorship Attribution Statement

Please select one of the following; *delete as appropriate:

*(B) This thesis contains material from 1 paper(s) published in the following peer-reviewed journal(s) / from papers accepted at conferences in which I am listed as an author.

Sections 2.2.2, 2.2.3, 2.2.4, 3.2.2, 3.2.3 is published as Tan, J.Y.; Zhang, Z.; Izzah, H.J.; Fong, Y.K.; Lee, D.; Mutwil, M.; Hong, Y. Volatile-Based Diagnosis for Pathogenic Wood-Rot Fungus *Fulvifomes siamensis* by Electronic Nose (E-Nose) and Solid-Phase Microextraction/Gas Chromatography/Mass Spectrometry. *Sensors* **2023**, *23*, 4538. https://doi.org/10.3390/s23094538

The contributions of the co-authors are as follows:

- I wrote the drafts of the manuscript. The manuscript was revised together with Dr Hong Yan.
- Dr Hong Yan provided the initial project direction, guidance, and suggestions to the methodology of the paper.
- I performed all the data synthesis, investigation and conducted data evaluation. Field investigation was assisted by Mr Zhang Ziteng, Ms Izzah Hazirah Junin.
- Dr Fong Yok King provided guidance to the methodology and validation of the project.
- Mr Daryl Lee provided the resources for field investigation and assisted in the review and editing of the manuscript.
- Dr Marek Mutwil co-supervised the project with Dr Hong Yan.

06/02/2024

. . . . . .

Date

. . . . . .

Tan Jhing Yein

Acknowledgements

Firstly, I would like to express my deepest gratitude to my supervisor, Dr Hong Yan, for providing valuable advice and unwavering support throughout this project. Special thanks to Dr Marek Mutwil for his guidance, as well as my FYP students, Izzah Hazirah Junin, Zhang Ziteng, Samuel Chee En Le for the support provided in the lab.

Secondly, the completion of the study could not have been possible without the indispensable expertise of Dr. Fong Yok King, and the NParks team for the identification of relevant pathogenic fungi-infected trees for sample collection. I would also like to thank Mr Steven Yuan and Mdm Wong at CMMAC MSLab for providing support with the GCMS analysis.

Lastly, I am grateful to my family for their support.

Table of Contents

Title: Volatile-based diagnosis for pathogenic wood rot fungi affecting Singapore urban trees

Abstract

The accurate and timely detection of fungal pathogens is crucial for effective wood rot disease management and prevention in Singapore urban trees. In this study, six species of wood rot pathogens – *Fulvifomes siamensis, Rigidoporus microporus, Pyrrhoderma noxium, Lasiodiplodia theobromae*, *Ganoderma orbiforme* and *Ganoderma australe* were studied. It was hypothesised that these species have distinct volatile profiles, and volatile-based detections tools - electronic-nose (e-nose) and solid-phase microextraction gas chromatography-mass spectrometry (SPME-GC-MS), can help identify these unique volatile profiles. This can be applied in the diagnosis of wood rot fungi in the field.

This thesis showed that the six different species had unique volatile profiles via SPME-GC-MS characterisation. A consistent, high-abundance volatile was identified for *F. siamensis* samples — 1,2,4,5-tetrachloro-3,6-dimethoxybenzene. The e-nose in its basic protocol is insufficient for disease diagnosis application. A new protocol was demonstrated with the introduction of nitrogen gas for purging sensor volatile residue. The purge enhanced the sensitivity of the e-nose sensors, allowing species-specific volatile profile differentiation. Additionally, the new protocol can be extended to distinguishing *in vitro* infection by *F. siamensis* and *R. microporus* fungi as early as two weeks post-treatment. This thesis also established a model that could assist in the identification of *F. siamensis* basidiocarps in real-time field diagnosis and validated with molecular identification by DNA barcoding. Overall, volatile-based detection shows promising applicability in the field of wood rot disease detection, and can achieve early-stage, fungus species specific diagnosis for wood decay.

Chapter 1: Introduction

Singapore's green initiatives began in 1967 during a period of rapid industrialization and urbanization with the incorporation of abundant green spaces within the urban landscape [1]. Through meticulous planning and dedicated implementation, Singapore transformed into a globally recognized "garden city" by the late 1980s. The country continued to expand its green spaces, resulting in a nationwide vegetation coverage of 49% in 2018 with a tree canopy coverage of around 30%, a 13% increase from 1986 [2]. This achievement positioned Singapore among the cities with the highest urban tree densities worldwide [3,4]. The city features various tree species along roadsides and in parks, including the Rain Tree (*Samanea saman*), Yellow Flame (*Peltophorum pterocarpum*), Casuarina (*Casuarina equisetifolia*), Angsana (*Pterocarpus indicus*), Broad Leaf Mahogany (*Swietenia macrophylla*), Senegal Mahogany (*Khaya senegalensis*), Trumpet tree (*Tabebuia rosea*), and Sea Apple (*Syzygium grande*). Urban trees in Singapore not only enhances the aesthetics of the environment, but also play a crucial role in carbon sequestration and countering climate change [5]. As such, Singapore has set a target to plant an additional one million urban trees by 2030, furthering their commitment to sustainability and green initiatives.

Singapore's tropical climate, characterized by high temperatures and humidity, provides favourable conditions for a wide range of plant species to thrive. However, this same climate also creates an environment conducive to the growth and spread of pathogenic fungi that cause wood rot. These fungi can possess oxidizing enzymes like hemicellulases, glucanases, laccase, lignin peroxidase, and manganese peroxidase that allow them to break down essential components of tree sapwood and reduce its resistance to secondary decay by other wood decay fungi [6]. As a result, the wood decay process leads to the formation of hollow trees which compromises the structural stability and integrity of trees. In addition, the live sapwood responds to fungal infection by compartmentalizing it, creating a protective barrier.

This allows for the continuous growth of healthy wood and bark on the outer layer, while the wood decay fungus continues to decompose the dead wood in the interior [7]. As a result, the initial phases of wood rot disease typically lack noticeable symptoms, while visible indications such as the emergence of fruiting bodies, crown dieback, and cavities typically manifest only in the later stages of infection [7-9].

Furthermore, these pathogenic fungi can persist in the soil alongside decaying wood remnants even after infected trees have been removed [10,11]. If the contaminated soil remains untreated, neighbouring healthy trees or newly planted trees can still become infected through contact with the pathogenic fungi that directly invade open wounds on the tree roots, trunks, and branches [12]. This poses a challenge to the sustainable management of urban trees, and it is thus crucial to develop suitable methods to diagnose or indicate the presence of the major pathogenic fungi that impact Singapore urban trees.

1.1 Studies on wood rot fungi

A survey of wood rot fungi in Singapore was published in the study by Hong et. al [13]. In the survey, 245 samples from 134 trees across 14 different tree species was sequenced through Illumina sequencing at the ITS1 region and the sequences were clustered into main Operational Taxonomic Units (OTU) (with 98% sequence similarity threshold). 17 pathogenic fungi were detailed in Hong et al. [13] to be the major cause of wood rot disease in Singapore urban trees. This was accomplished by determining their significant presence in diseased tissues, along with their concurrent presence in soil and/or fruiting bodies and were further evidenced by *in vitro* wood loss studies. Majority of the fungi belonged to the phyla of Ascomycota (63.3%) and Basidiomycota (22.5%) [13].

Ascomycota is widely known for its economic importance in the medical (e.g. Penicillium for antibiotic production), food and beverage industries (e.g. *Saccharomyces cerevisiae*, which is

used in baking, brewing, and winemaking). However, certain species of the Ascomycota phylum such as the Hypoxylon species which have been reported to cause wood rot in tea cultivars [14] and Xylaria species that commonly cause white rot disease which degrades lignin in the tree wood tissues [15]. Basidiomycota fungi are involved in the ecological processes as decomposers that break down wood and plant debris that contributes to nutrient cycling in the ecosystem. Many basidiomycetes decay only dead wood (saprophytes), while some are capable of breaking down complex lignocellulosic materials in living trees (parasites) [16]. When a parasitic fungus enters a living plant via an exposed wound, it may lead to wood rot disease.

The main OTU clustering data, generated by Hong et al. [13] and summarised in Figure 1, revealed that fungi from the orders Polyporales and Hyemenochaetales, under the Basidiomycota phylum, were detected in large abundance in the surveyed samples. Notably, these two orders include many wood decay fungi that are commonly known as polypores or bracket fungi. These fungi are characterized by their formation of fruiting bodies with a distinctive pore surface on the underside, from which they release spores.

Out of the 17 species reported by Hong et al. [13], this thesis further shortlisted five Basidiomycota pathogenic fungi: three Polyporales (*Rigidoporus microporus, Ganoderma orbiforme* and *Ganoderma australe*) and two Hyemenochaetales (*Fulvifomes siamensis* and *Pyrrhoderma noxium*), that were found recurring across multiple tree samples from more than one host tree species, with high total abundance sequence counts. Additionally, *Lasiodiplodia theobromae* from the Ascomycota phylum of Dothideomycetes class that was isolated from two different diseased wood tissue sample was also selected as a representative of the Ascomycota phylum. The following subsections would list more details on each of the six shortlisted wood rot pathogens.

Figure 1: Taxonomic distribution of fungi species from the survey of 245 samples based on metagenomic analysis of ITS1 region reads and absolute counts. Data from Hong et al. [13].

1.1.1 Fulvifomes siamensis

Fulvifomes is a monophyletic genus within the Hymenochaetaceae with 49 species recorded [17]. Fulvifomes shares a phylogenetic relationship with Phylloporia and Flaviporellus, with all three genera characterized by the absence of setae and the presence of a thick basidiospores. Phylloporia exhibits parasitic properties and grow on living plants, Flaviporellus basidiocarps (fruiting body) have been reported to grow on dead wood [18], and turn deep red in reaction with potassium hydroxide (KOH). While Fulvifomes commonly thrives on dead wood, some have been found to inhabit living trees and induce white rot, and its basidiocarps turn black-brown in reaction with KOH [17].

F. siamensis was initially identified in a survey of stem or butt rot of *Xylocarpus granatum* trees at Hat Khanom-Mu Ko Thale Tai National Park in Thailand by Sakayaroj et al. [19,20]. The basidiocarp is identified to be perennial, have a semi-circular pileate (have a cap-like structure) with varying texture as they age from velutinate (velvety) to glabrous (smooth) to rimose (cracked). The pileate is hard and turns from yellow-brown to brown-black in older specimens and do not have a distinct crust. Their basidiospores are subglobose (almost spherical), yellow-brown, and slightly thick-walled [20] (Figure 2). *F. siamensis* is inferred to share phylogenetic relations with *F. fastuosus* and *F. nilgheriensis*, but differ in their pileus surface structure as the latter two species have a distinct crust [20].

In Singapore, *F. siamensis* was also observed to have a high degree of morphological plasticity, indicating that its physical characteristics can vary widely depending on the specific developmental stage and the type of tree it infects. The observed variations in *F. siamensis* encompassed a range of characteristics, such as colour (spanning from orange, brown, to black), the presence or absence of white fringes, and diverse shapes (including clumps, multi-layered forms, and flat fan-like structures) [13]. This morphological plasticity of *F. siamensis* presents a challenge to the identification and diagnosis of the fungus solely based on visual assessments and morphology. Due to the wide presence of *F. siamensis* in multiple different Singapore urban tree species [13], it was chosen as a focus species for downstream experiments for volatile-based diagnosis.

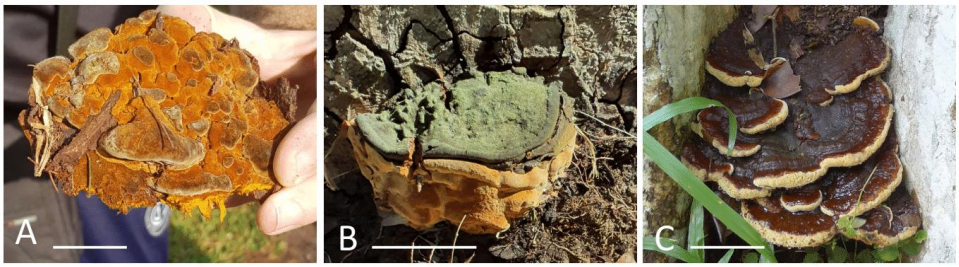

Figure 2: *Fulvifomes siamensis* found in Singapore. A: Orange-brown, velutinate basidiocarp of *F. siamensis* from a Casuarina tree; **B**: Yellow-brown, rimose basidiocarp of *F. siamensis* from a Khaya tree; C: Brown, glabrous basidiocarp of *F. siamensis* from a *Syzygium grande* tree. Scale bars are 5 cm. Photos credit: Hong et al [13].

1.1.2 Rigidoporus microporus

Rigidoporus genus belongs to the order Hymenochaetales and family of Meripilaceae, contains over 40 known species [21], and commonly grow on angiosperm and gymnosperm wood [17]. Rigidoporus is phylogenetically related to Oxyporus, with the former characterised by having basidiocarps with a coloured pore surface, thick-walled encrusted hyphoid cystidia (specialised structures), and mammillate cystidioles, while the Oxyporus species are associated with light-coloured basidiocarps and thick-walled encrusted hymenial cystidia [22].

R. microporus typically form large, perennial basidiocarps with a red-brown colouration, and its pileal surface is glabrous. When dry, the pileal surface becomes distinctly segregated into concentric rings (zonate) and grooves become inherent (sulcate) [22]. The upper surface of the fruiting body is usually smooth or finely hairy, while the pore surface is porous and yellow-brown (Figure 3). In Singapore, *R. microporus* was initially discovered as a pathogenic fungus of *Hevea brasiliensis* (rubber tree) in the Singapore Botanic Gardens in 1904 [23]. Further studies confirmed that *R. microporus* could cause white rot disease and primarily affected the root systems of a wide range of tree species from hardwoods, conifers to food and cash crops [10,21]. It can cause significant damage and decay in the roots, leading to the weakening and eventual death of the host tree, hence regarded economically important to African and several South East Asian countries such as Malaysia, Thailand and Philippines [21,24,25].

Figure 3: *Rigidoporus microporus* found in Singapore. A: Red-brown, glabrous basidiocarp of *R. microporus* from a Rain tree; **B**: Orange-brown, zonate, and glabrous basidiocarp of *R. microporus* from a Palm tree stump. Scale bars are 5 cm. Photos credit: Hong et al [13].

1.1.3 Pyrrhoderma noxium

Pyrrhoderma noxium, also named formerly as *Phellinus noxius,* was recently reclassified into the genus Pyrrhoderma with contains a total of 7 species [26] and belongs to the Hymenochaetaceae family. In terms of phylogeny, Pyrrhoderma is closely affiliated with Cylindrosporus, a monotypic genus that originated from Onnia. Both Pyrrhoderma and Cylindrosporus have annual, sessile basidiocarps, and thin-walled basidiospores. However, Cylindrosporus has hymenial setae (hair-like structures on the spore-bearing surface of the fungi), while Pyrrhoderma has hyphoid setae (hair-like structures located away from the hymenium) [27].

The upper surface of the *P. noxium* basidiocarp changes from yellow-brown with white borders, to brown, to dark grey as it ages [8] (Figure 4). It has been reported to be widely distributed worldwide, ranging from tropical regions of Southeast Asia, the Pacific Islands, to regions in Japan, Taiwan, Australia, Central America, and Africa [28]. *P. noxium* has been widely studied for causing brown root rot disease and has been identified as a major threat to over 200 hardwood and softwood tree species. Reports of tree with brown rot disease caused by *P. noxium* are rampant in Taiwan [8,29] and in tree plantations of Malaysia [25,30]. *P. noxium* commonly forms a distinctive brown mycelial layer (known as the mycelial mat) on the outer surface of infected trees' bark, as reported by Hodges and Tenorio in 1984 [31] and Chang et. al [32]. Internally, the root tissues would initially turn brown, followed by white and soft, accompanied by the presence of the dark brown mycelia lines throughout the affected tissue [29]. The progression of the disease leads to symptoms such as chlorosis (yellowing) and defoliation as the fungus impairs the trees' root function. Usually, aboveground symptoms are not noticeable until significant root damage has occurred.

Figure 4: *Pyrrhoderma noxium* found in Singapore. 4A: Brown-black, glabrous basidiocarp with white edges of *P. noxium* from a tree log; **4B**: Dark gray, velutinate basidiocarp of *P. noxium* from a fallen tree branch; C: Bark area of a Khaya tree with *P. noxium* mycelia. Scale bars are 5 cm. Photos credit: Hong et al [13].

1.1.4 Ganoderma sp. (G. orbiforme and G. australe)

The genus Ganoderma is part of the class of Agaricomycetes, in the Polyporaceae family which encompass around 278 species of fungi with a glossy and stalked basidiocarp [33]. The genus was established in 1881 with *Polyporus lucidus* (currently known as *Ganoderma lucidum*) as the generic type [34]. The Ganoderma species are ecologically and economically significant species, serving roles as producers of medically important metabolites. However, these species are also identified to cause white rot fungi that target the heartwood of tree trunks and degrade the cellulose and lignin components. One of the characteristic signs of Ganoderma wood rot is the presence of large, perennial basidiocarps with woody texture, with a distinctive bracket-like appearance. The surface is usually smooth, with a glossy or matte texture, and can have different colours, including shades of brown, red, or black. Affected tree species include *Acacia mangium* trees [35] and palms [36].

G. orbiforme was initially identified and documented under the name *Polyporus orbiformis,* based on the initial specimen obtained from Guinea, Africa [37]. It has further been recorded to be found in several countries in Asia [38]. The fungus has annual or perennial, sessile basidiocarps, and the pileus surface is weakly laccate (lacquered appearance) in certain areas, a brown context, brown pore surface, and a brown tube layer (Figure 5A). Additionally, it produces ellipsoid or ovoid basidiospores. A research done on oil palm (*Elaeis guineensis*)

plantations in Malaysia identified three Ganoderma species - *G. boninense* (also known as *G. orbiforme*), *G. zonatum*, and *G. miniatocinctum* which are responsible for causing basal stem rot disease [39].

G. australe was first identified from the Pacific Islands, and is part of the *Elfvingia* subgenus [40]. They have annual or perennial, subdimidiate (fungal cap not completely attached to the stem), and sessile basidiocarps. The pileus is often in hues of brown or red-brown, and the surface can range from being smooth during active development stages, to a hard and non-laccate (dull) at the mature stage [41] (Figure 5B). *G. australe* causes white rot in a variety of hosts worldwide, especially in tropical forests [42] and has been reported to affect ornamental trees such as Tower tree (*Schizolobiuni parahybum*) in Malaysia [43].

Figure 5: *Ganoderma* species found in Singapore. A: Brown basidiocarp with white edges of *G. orbiforme* from a Yellow Cane palm; **B**: Dark brown, non-laccate basidiocarp of *G. australe* from a Yellow Cane palm. Scale bars are 5 cm. Photos credit: Hong et al [13].

1.1.5 Lasiodiplodia theobromae

Lasiodiplodia belongs to the family Botryosphaeriaceae and class Dothideomycetes, with its first typified species *L. theobromae* [44]. The family is distinguished by its large, oblong, usually translucent (hyaline) and aseptate (lack cell walls) ascospores (sac-like sexual spores of Ascomycetes). Their conidia, asexual spores, can be either hyaline or pigmented, usually aseptate and thick-walled [44]. Additionally, Lasiodiplodia have unique presence of pycnidial paraphyses, which are asexual reproductive structures amongst the sterile cells, and longitudinal striations on the mature conidia. These asexual characteristics of Lasiodiplodia allows differentiation from other closely related genera in the family. Lasiodiplodia species

are distributed globally in tropical and subtropical regions, displaying a broad host range of monocots, dicots, and gymnosperms. These species can be endophytic, reside in asymptomatic plant tissues, act as saprobes on deceased plant matter, or cause disease in living hosts [45].

L. theobromae is a fungal pathogen that has a diverse range of hosts including fruit trees, ornamental plants, and agricultural crops, leading to significant economic losses to plantations with *Theobroma cacao* [46], *Jatropha curcas* [47] and Mulberry [48]. The fungus can infect different parts of the plant, including stems, branches, leaves, and fruits and cause various diseases including fruit rot, stem cankers, black root rot and dieback [49]. During the infection process of *L. theobromae*, the affected plant parts develop dark brown-black lesions which may expand over time, causing extensive tissue necrosis. Cultures of *L. theobromae* are initially display grey, fluffy mycelia within four to five days of incubation, before turning black after 14 to 15 days of incubation [48] (Figure 6).

This species would aim to serve as a representative from a different phylum (Ascomycota) in comparison with the other five Basidiomycota species utilised in this thesis for volatile analysis.

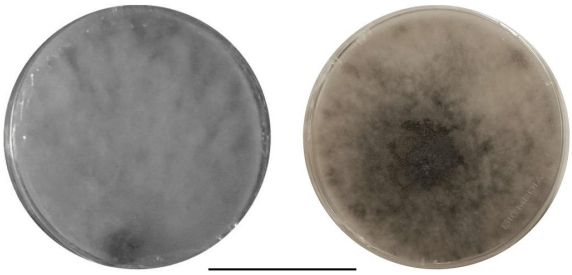

Figure 6: *Lasiodiplodia theobromae* cultures isolated on 2.4% potato dextrose agar media. A: Grey mycelia of *L. theobromae* after 7 days of incubation; **B**: Mycelia of *L. theobromae* turning black after 14 days of incubation. Scale bar is 5 cm.

1.2 Studies on volatile-based diagnosis (e-nose and SPME-GC-MS) of tree diseases

Diagnosis of plant diseases typically involves analysing wood tissues and soil samples using molecular techniques such as DNA extraction and polymerase chain reactions (PCR). These methods provide specific and sensitive results [50]. However, they are expensive and require time for analysis [51]. Moreover, conducting PCR-based diagnosis necessitates specialized expertise and a specific laboratory analysis, making them time-consuming and expensive. Sampling is also invasive and creates wounds that may introduce new infection. Hence, there is a need for cost-effective and rapid alternative diagnostic solutions to identify wood rot fungal infection in trees.

Plants emit volatile organic compounds (VOCs) in response to various factors, including their physiological health, age, microbial pathogen infections [52], and interactions with the environment (such as light, temperature, and humidity) [53,54]. These VOCs can include isoprenoids, benzenoids, fatty acid derivatives, and amino acid derivatives [52,55]. Similarly, fungi release a variety of VOCs as part of the products of their primary and secondary metabolism, such as aldehydes, alkenes, alcohols, ketones, benzenoids, carboxylic acids, and isoprenoids. Detection and identification of these specific VOCs emitted by fungi have the potential utility for identification [56].

Using volatile organic compounds (VOCs) for diagnosis offers significant benefits compared to traditional molecular-based methods. VOC sampling allows for the differentiation of specific samples infected with fungi, without causing damage or reducing the value of the sample materials. VOC-based diagnosis can also be cost and time-effective. Furthermore, machine learning algorithms have the potential to be trained in order to achieve greater discrimination between different categories of pathogen-infected samples [57].

1.2.1 E-nose

The fundamental principle behind the functioning of an electronic nose (e-nose) lies in the alteration of resistance and electrical conductivity of its sensors when they come into contact with gas-phase analytes. These analytes can belong to various chemical classes or possess different functional groups. By using a set of sensors with varying specificity for different chemicals, an e-nose generates a distinct response profile that enables the differentiation of different volatile samples.

Application of the e-nose was used to detect of harmful strains of *Fusarium verticillioides*, a fungus known to cause various diseases in corn, including stalk rot, ear rot, and kernel rot, and cause contamination of the crop as they produce harmful mycotoxins, such as fumonisins, that poses risks to human and animal health if consumed [58]. The authors used an e-nose equipped with metal oxide semiconductor (SMO) sensors which was able to differentiate the presence of toxigenic *Fusarium* strains in maize samples from the healthy samples. Another study by Baietto et al. showed promising results using a commercial portable SMO e-nose, PEN3, to differentiate healthy shade tree species from those infected with root rot fungi *Armillaria mellea (Vahl) P. Kumm*, *Ganoderma lucidum (Curtis) P. Karst*, and *Heterobasidion annosum* after a 12-month incubation [59]. Additionally, the authors observed that the different types of root rot pathogens emitted distinct VOC patterns, suggesting that the e-nose could have the potential to not only detect the presence of root rots but also potentially differentiate between different causative agents.

1.2.1.1 Cyranose® 320

In this thesis, a commercial e-nose, the Cyranose® 320 (Smiths Detection, Inc., Pasadena, CA, USA) (Figure 7), was used for the e-nose analysis. The sensing element of the Cyranose 320 device consists of the NoseChip™, which is comprised of an array of 32 chemi-resistor sensors made of polymer composites [60]. These sensors are coated with conductive films and

arranged across electrodes. The Cyranose 320 device incorporates two separate pathways for gas measurement: the "Purge Inlet" path, which draws in a baseline gas (typically ambient air) to measure the R_o value, and the "Sample Inlet" path, which draws in the volatile organic compounds (VOCs) from the analyte to measure the R_{max} value. The device measures the voltage change, with formula $\Delta R/R_o = (R_{max} - R_o)/R_o$, across each sensor in the array, and this change is converted into a resistance reading. The conductive pathways of the device will return to their original state once the analyte is purged with, typically, ambient air.

Figure 7: Cyranose 320 e-nose. [61]

The resistance readings are then analysed using an onboard unsupervised machine learning algorithm called Canonical Discriminant Analysis (CDA). This would help to classify the samples' volatile profiles in a dimensional reduction form via a Principal Components (PC) plot, visualised either two- or three-dimensionally.

The Cyranose 320 has a competitive advantage over other e-nose like the Sacmi EOS507C due to its portability and ease of operational use in the field. In comparison to other portable commercial e-nose like the AirSense PEN3 metal oxide sensor, the Cyranose 320 has more sensors (32 versus 10), and its carbon polymer sensors have higher sensitivity to lower volatile concentrations as compared to metal oxide sensors [62]. Furthermore, multiple studies on plant pathogen identification were done on the Cyranose 320 [63].

The Cyranose 320 has been studied in terms of its usage in the fields of medical diagnosis, such as the volatile classification of six species of bacteria that are known to cause eye infections [64], as well as in the food quality control industry, such as the use of the e-nose to differentiate varying quality of olive oil [65]. With more relevance to the study on fungal wood decay in plants, the Cyranose 320 was demonstrated by Markom et al. to discriminate between healthy and basal stem rot fungus *Ganoderma boninense*-infected oil palm trunk and soil samples [66]. Prior studies from Final Year Reports of Tan (2021) [67] provided concept proof that the Cyranose 320 could assist in differentiating plant and fungi-related chemical volatiles, and among fungal mycelia cut plugs of *F. siamensis, R. microporus* and *P. noxium,* at varying incubation period of one day and three days with ambient air as the baseline gas.

1.2.2 SPME and GC-MS

Solid phase microfiber extraction (SPME) is a sampling method that involves the use of microfiber instead of solvents for the extraction of volatile compounds in a non-exhaustive manner [68]. It requires a smaller amount of analyte compared to traditional solvent-based extractions [69]. Upon heating in sample chamber, the microfiber releases the extracted analytes, which can then be subjected to GC-MS analysis which allows for the identification and quantification of each volatile compound.

Volatile-based detections in plant material with gas chromatography mass spectrometry (GC-MS) have been demonstrated on potato tubers infected with *Phytophthora infestans* (which causes late blight disease) and *Fusarium coeruleum* (which causes dry rot) [70]. Volatiles were identified to be present in high abundance for both pathogens include benzothiazole and 2-ethyl-1-hexanol and were not found to be emitted by the healthy samples. In the case of *Phytophthora infestans*-inoculated samples, specific VOCs such as butanal, 3-methylbutanal, undecane and verbenone were identified at low amounts, while *Fusarium coeruleum*-inoculated samples showed the presence of compounds like 2-pentylfuran and 2-

ethylhexanal. These VOCs could potentially serve as biomarkers for the early detection and differentiation of the two pathogens. Prithiviraj et al. [71] also utilised GC-MS to identify and analyse the volatile metabolites emitted by post-harvest onion bulbs after a three or six day inoculation with *Erwinia carotovora ssp. carotovora*, *Fusarium oxysporum*, and *Botrytis allii*. The results revealed distinct profiles of volatile metabolites for each pathogen-infected bulb, indicating the presence of specific compounds associated with each infection. For instance, *B. allii*-inoculated samples produced unique metabolites acetone, 1-(methylthio)-E-1-propene, and 1-ethenyl-4-ethylbenzene in relatively high abundance; while *F. oxysporum*-inoculated samples produced 1-Oxa-4,6-diazacyclooctane-5-thione in relatively high abundance.

1.2.3 Combined usage of e-nose and SPME GC-MS

A study done by Loulier et al. [72] investigated the effectiveness of both the e-nose and SPME-GC-MS in differentiating the volatile profiles of various species of fungi and oomycetes. The e-nose was found to be able to distinguish between four fungal species, *Phytophthora ramorum, Fusarium poae, Trichoderma asperellum* and *Rhizoctonia solani*, from the control samples, whereas the use of SPME-GC-MS provided detailed information about the specific volatile compounds associated with each species. The combination of these techniques enhanced the overall detection capability and reliability of the e-nose detection.

While the e-nose has been established by prior works of Markom et al. [66] to be capable of qualitatively distinguishing between healthy and wood-rot fungi infected samples, specific volatile molecules accountable for clustering and differentiation remained unidentified as the e-nose primarily focused on pattern recognition rather than providing specific information about the identity and quantity of VOCs present in the samples. Hence, this thesis explores the complementary usage of the e-nose and SPME GC-MS to distinguish and quantify the volatiles in the species-specific detection of wood rot fungi in diseased tree samples.

Studies on the practical application of the e-nose for use in the real-world settings for the detection of wood rot diseases in urban tree species are also limited.

For practical applications in the field setting, there is a potential issue regarding the influence of various air compositions in the operational environments, including air contaminants originating from vehicles and industrial emissions [73]. These external factors may introduce additional volatile compounds that could mask the detection of pathogenesis-related volatiles. Hence, this thesis aims to develop an optimised protocol and validate the e-nose in the practical application in actual field studies.

1.3 Overarching hypothesis

Wood rot fungi infection is hypothesised to generate a unique profile of VOCs that can be used for disease diagnosis through volatile-based detection tools. Volatiles released by the fungi or the host tree metabolism, or through fungi-host interactions, can possibly be detected by commercially available tools. If the above hypothesis is true, these volatile-based techniques could then be used to provide reliable diagnostic results on top of current practices of tree visual assessments which are either ineffective for early stage diagnosis or are inaccessible in the field and costly.

Firstly, volatiles of the various fungi pathogen cultures purified in the lab were analysed to identify unique volatile patterns. Secondly, pathogenicity of these fungi pathogens was tested on wood blocks of Singapore urban trees to demonstrate early stage infection *in vitro*. Volatile profiles of these samples were then analysed to determine if the volatile-based techniques are capable of distinguishing healthy and fungi-exposed samples at the early stage of the disease. Lastly, the volatile-based diagnosis was tested for its applicability in the field to detect wood rot fungi in a species-specific manner.

Chapter 2: Species-specific volatile pattern recognition and profiling

This chapter shows that volatiles can be classified by their unique VOC patterns with good sensitivity and specificity using an improved protocol for the e-nose analysis with nitrogen gas. In this thesis, sensitivity is defined as the ability to differentiate the samples from the control (i.e. the fungi samples from the non-fungi samples; plant/fungi-related volatiles from air), while the specificity is defined as the ability to distinguish every unique sample apart (i.e. fungi species-specificity; different plant/fungi-related volatiles). The sensitivity and specificity of the e-nose was tested through analysing plant and fungi-related volatiles, namely acetic acid, turpentine, and farnesene. Acetic acid (CH_3COOH) is a type of monocarboxylic acid that has been documented as an intermediate product formed during the degradation of cellulose by fungi that cause wood decay [74]. Turpentine ($C_{10}H_{16}$) is a mixture of unsaturated hydrocarbon terpenes, predominantly alpha-pinene and beta-pinene, commonly found to be emitted by coniferous trees. Farnesene ($C_{15}H_{24}$) is a mixture of isomeric sesquiterpenes, that can be released by several tree species like Douglas fir [75].

Secondly, to test species-specific diagnosis using volatile-based techniques, volatile profiles given out by pure isolates of the six pathogens, *F. siamensis*, *R. microporus*, *L. theobromae*, *P. noxium*, *G. orbiforme*, and *G. australe* were identified via SPME-GC-MS and analysed with the revised protocol of e-nose/CDA classification. Furthermore, added soil tests to the mycelia cut plugs were conducted to determine if soil samples were feasible as a sample type for volatile tests.

2.1 Methodology

This methodology section outlines the comprehensive approach used in this study, starting with the foundational settings and algorithms of the Cyranose 320 e-nose and the accompanying statistical methods, as described in subsections 2.1.1 and 2.1.2. Specific

procedures used for volatile analysis with the e-nose, focusing on air samples from various locations and the refinement of testing protocols using plant- and fungi-related chemical volatiles, were detailed in subsections 2.1.3 and 2.1.4, respectively.

Subsection 2.1.5 covers the methods employed for collecting and processing wood rot fungi samples. The preparation and processing of fungal cultures, along with DNA extraction from the collected samples, are thoroughly explained in subsection 2.1.6. Following this, subsection 2.1.7 describes the barcoding and identification techniques used for these samples. Finally, subsections 2.1.8 details the steps for the e-nose analysis on volatiles from the prepared fungal cultures. Subsection 2.1.9 then discusses the utilization of SPME-GC-MS for a similar purpose, providing a comprehensive approach to the volatile analysis.

2.1.1 Cyranose 320 e-nose method settings

The settings for the Cyranose 320 method were derived from the Sensigent practical guide [60] and are presented in detail in Table 1. Prior to each run session, the Cyranose 320 e-nose would undergo an internal sensor pre-warming step after power-on for 5 min at 42 °C. For experiments using nitrogen gas as the e-nose baseline, 99.99% pure nitrogen gas was filled into refillable 3 L multi-layer gas sample bags (Jensen Inert Products, Coral Springs, FL, USA) and secured to the e-nose purge inlet valve with an airtight seal during the "baseline purge" phase. Samples were incubated inside Glad® Zipper Bags for a specified duration (e.g. 15 min), after which the 1.2 mm × 40 mm snout sampling needle of the Cyranose 320 was inserted into the bag, stopping approximately 2 cm away from the sample material. Following the measurement, the sample resistance readings data were downloaded and subjected to CDA Canonical graph plotting using Chemometric Data Analysis Program (CDAnalysis) software version 11.2.

Table 1: E-nose sampling method settings

Steps	Time (sec)	Pump Speed
Baseline purge	10	Medium (120 mL/min)
Sample draw	10	Medium (120 mL/min)
Air intake purge	5	High (180 mL/min)
Sample gas purge	30	High (180 mL/min)

2.1.2 Sampling algorithm and statistical analysis: Principal Component Analysis (PCA), Canonical Discriminant Analysis (CDA) and Interclass Mahalanobis distance (MDist)

CDA is a valuable unsupervised machine learning algorithm that enables the classification of samples into distinct classes within a lower-dimensional discriminant space based on the variation of multiple independent variables [76] . During the cross-validation process, the $\Delta R/R_o$ data captured form the 32 sensors are calibrated and dimensional reduced via Principal Component Analysis (PCA) to ten Principal Components (PC) (unless stated otherwise), which condenses the $\Delta R/R_o$ data from the sensor factors that capture the highest variance in the dataset and provides a visual representation on the classification of the samples based on their volatile patterns. To mitigate the impact of varying volatile concentrations and sampling techniques on the sample volatile profile, data processing utilizing the 'Normalisation 1' tool with auto-scaling was employed in this study [61].

The Interclass Mahalanobis distance (MDist) quantifies the correlation between data points belonging to two sets of sample classes. A MDist score greater than 5.000 signifies that the two sample classes are distinct and dissimilar, whereas a score below 5.000 indicates that the two sample classes are indistinguishable [61]. The software CDAnalysis version 11.2 was used to generate Canonical graph scatter plots and calculate the MDist scores based on the sensor resistance data obtained from the Cyranose 320. "Active sensors" were identified to significantly contribute to the PC axes of the Canonical graph if they collectively account for a minimum of 90.0% of the total variance. The average response data ($\Delta R/R_o$) of the active sensors is then plotted, with error bars representing the standard deviation.

2.1.3 E-nose analysis of air from various locations

To show the inconsistency of volatile reading patterns across ambient air samples at different locations, e-nose analysis was conducted on air samples obtained from six different locations. Air samples were collected using Glad® Quart Zipper bags measuring 17.4 cm x 19.3 cm (Glad Products, Oakland, CA, USA), with approximately 500 mL of air collected per sample. The specific locations from which the air samples were obtained were detailed in Table 2. Nitrogen gas was used as the baseline gas during the e-nose analysis of the six samples.

Table 2: Various location of air composition tested with details on the geographical GPS coordinates

Location ID	GPS Coordinates	Remarks
A	1°20’41.7”N 103°40’47.5”E	Cafeteria
B	1°20’40.4”N 103°40’43.5”E	Bus stop with vehicle traffic
C	1°20’50.6”N 103°40’46.2”E	Along a road undergoing construction works
D	1°20’39.6”N 103°40’45.7”E	Along a laboratory corridor
E	1°20’39.6”N 103°40’45.7”E	Inside the biosafety cabinet
F	1°20’39.6”N 103°40’45.7”E	Inside an office cubicle
G	1°20’40.5”N 103°40’46.9”E	An outdoor open area with vehicle (G1) and human traffic (G2)

2.1.4 E-nose analysis of plant and fungi-related reference VOCs

In a biosafety cabinet (Table 2, location E), a control sample was first prepared by placing a 2 × 2 × 0.04 cm L-fold paper towel (PT Suparma, Tbk, Surabaya, Indonesia), without any chemical products, into a Glad® Freezer Gallon Zipper Bags measuring 26.8 cm x 27.3 cm (Glad Products, Oakland, CA, USA). The sample bag was inflated to hold approximately 2 L of air, sealed. Aliquots of turpentine, farnesene, and acetic acid were applied to the same sized 2 × 2 × 0.04 cm L-fold paper towel to achieve various concentrations of volatile compounds ranging from 0.05 ppm to 5.0 ppm. These paper towels were similarly placed

inside Glad® Freezer Gallon Zipper Bags and were inflated to contain 2 L of air in the biosafety cabinet. Sample bags were left to sit for 15 min before the e-nose analysis. It was assumed that complete evaporation of the VOCs would occur during the 15 min sample incubation to reach the desired concentrations. Measurements of the samples were conducted in a controlled environment of an office space (Table 2, location F) using either the ambient location air or nitrogen as the baseline purge gas for e-nose analysis.

2.1.5 Sample collection, processing, and DNA isolation

Collected samples from trees with fruiting bodies include both the basidiocarp and the cambium or sapwood from areas where decay was detected, to assess the presence of fungi in the wood tissue, as well as healthy wood pieces. Records on the collected samples include the location, collection date, host tree species and morphology, and photos with size references.

To extract DNA from the fruiting bodies and wood tissue samples, a sterile hand saw was used to slice open the samples and cut smaller sample fragments from the freshly exposed inner parts. These fragments were subsequently ground with a mortar and pestle in liquid nitrogen. From the powdered fragments, 100 mg was taken and utilized for DNA isolation using the Qiagen DNeasy Plant Pro kit (Qiagen, Hilden, Germany), following the manufacturer's protocol.

2.1.6 Fungal culture preparation and mycelia DNA isolation

Small fragments from the interior of collected fruiting body and tissue samples obtained as detailed in section 2.1.5 were plated onto 2.4% potato dextrose agar (PDA) media supplemented with antibiotics (streptomycin 30 mg/L + ampicillin 100 mg/L), with the culture plates measuring 90 mm diameter (Biomedia, Singapore). To obtain pure cultures, the hyphae at the edge of the colonies that grew from the fragments were sub-cultured onto new PDA plates using a sterile scalpel blade. The plates were incubated in a dark environment at

30 °C to facilitate fungal growth. The lyticase-chelex 100 DNA isolation protocol for fungal mycelia as detailed in Pryce et al. [77] was used.

2.1.7 Sample barcoding and identification for fruiting body and fungal culture samples

PCR amplification was conducted on the DNA isolated from the fruiting body and fungal mycelia, targeting the ITS1-5.8S-ITS2 region using the V9D (5'-TTAAGTCCCTGCCCTTTGTA-3') [78] and LS266 (5'-GCATTCCCAAACAACTCGACTC-3') primer pair [79]. The PCR program consisted of an initial denaturation step at 95 °C for 5 min, followed by 35 cycles of denaturation at 95 °C for 30 sec, annealing at 50 °C for 30 sec, and extension at 72 °C for 30 sec. A final extension step was performed at 72 °C for 5 min [77]. The PCR amplicons were purified using the QiaQuick PCR purification kit (Qiagen, Hilden, Germany) before being sent for Sanger sequencing (Bio Basic Asia Pacific Pte Ltd., Singapore) with ITS5 (5'-GGAAGTAAAAGTCGTAACAAGG-3') and ITS2 (5'-GCTGCGTTCTTCATCGATGC-3') primers. The forward and backward sequences were assembled to obtain a consensus sequence via Geneious Prime (version 2022.0.1). NCBI BLAST search was then conducted to obtain the sample molecular identity with the best match result and lowest E value (less than 1e-100).

Isolated DNA of selected fruiting body and diseased tissue samples that gave mixed trace signals (multiple sequence peaks at the same location) from the results of Sanger sequencing were subsequently sent for ITS1 Amplicon Metagenomics Sequencing using the Illumina NovaSeq PE250 sequencing platform with 50K tags per sample (NovogeneAIT Genomics, Singapore) as detailed in Hong et al [13].

Briefly, the DNA was amplified using Phusion® High-Fidelity PCR Master Mix (New England Biolabs, Ipswich, MA, USA) with primer pairs ITS5 and ITS2. The library was

generated with NEBNext® UltraTM DNA Library Prep Kit (New England Biolabs, Ipswich, MA, USA). FLASH (V1.2.7) was employed to merge the paired end reads and generate raw tags. Fastp and Vsearch software was used to filter out low-quality tags and align the clean tags with a database respectively. For taxonomic classification, the DADA2 module within the QIIME2 software was mostly utilized to obtain Amplicon Sequence Variants (ASVs) of the final effective tags of each sample, and the Classify-sklearn module was employed to compare ASVs with the Fungi Unite database (https://unite.ut.ee, accessed on 31 January 2023), resulting in the species annotation for each ASV. Subsequently, clustering was performed on the ASVs using sumaclust (Version 1.0.36) (https://git.metabarcoding.org/obitools/sumaclust/-/wikis/home, accessed on 31 January 2023) through Spyder Python 3.9 software (https://www.spyder-ide.org/, (accessed on 31 January 2023) with a threshold of 98.0% sequence similarity. The representative sequence from each cluster was determined as the sequence with the highest sum of all pairwise similarity scores. These representative sequences were designated as the main operational taxonomic units (main OTU).

2.1.8 E-nose analysis of fungal mycelia volatiles

Following the fungal culture preparation in 2.1.6 and pure fungal identity confirmation through Sanger sequencing in 2.1.7, a fresh culture plate was prepared by sub-culturing one cut plug of the selected species (Table 3) onto a 90 mm culture plate with 2.4% potato dextrose agar (PDA) media supplemented with antibiotics (streptomycin 30 mg/L + ampicillin 100 mg/L).

Table 3: Fungal cultures of the selected wood rot species for volatile-based analysis

Species	Fungal Culture in 2.4% PDA medium	GenBank Accession No.
F. siamensis		OQ618213
R. microporus		OQ558869
L. theobromae		OQ558857
P. noxium		OQ558864
G. orbiforme		OQ558852
G. australe		OQ558853

To create cut plugs of the fungal mycelia, the 8 mm diameter end of a sterile 1000 µL micropipette tip was used to cut into the pure cultures, containing approximately 3.67 mg of fresh mycelia. The cultures were incubated for ten days before they were used for the volatile-based analysis.

For the volatile-based analysis, varying numbers of cut plugs (denoted as −5, −10, −15, for five, ten, and fifteen cut plugs, respectively) were transferred into a Glad® Quartz-sized Zipper Bag (Glad Products, Oakland, CA, USA), which was then inflated and sealed in the biosafety cabinet to contain 500 mL of head space. A control sample, with only 2.4% PDA media with antibiotics was also used. The samples were incubated for 15 min in a dark environment at room temperature before e-nose analysis with six readings per sample and with nitrogen used as the baseline gas. The e-nose method settings and downstream evaluation with Canonical Discriminant Analysis (CDA) were as described in subsection 2.1.1 and 2.1.2.

For *F. siamensis, P. noxium, R. microporus,* and a control sample of only 2.4% PDA with antibiotics, ten cut plugs were placed in 10 g of sieved sterile garden soil that was autoclaved at 121 °C for 15 min to determine if the presence of soil could affect the e-nose sensitivity and specificity. These samples with added soil are indicated with suffix -S1 and -S2 (indicating replicates) and were incubated for three days to allow the fungi to acclimatise and grow in the new soil environment.

2.1.9 SPME-GC-MS of fungal mycelia volatiles

For selected cut plug samples, six cut plugs were placed into a 20 mL clear vial capped with 20 mm Viton® Septa Seals (Supelco Inc., Bellefonte, PA, USA). Some samples with 1 g of sieved autoclave soil and one cut plug were also sealed in the same manner. Solvent-free sampling of analytes was performed using a divinylbenzene/PDMS/Carboxen-coated fiber

with dimensions of 50/30 μm securely housed within a protective needle, which was then attached to a manual SPME holder. To conduct the sampling, the fiber assembly was inserted into the sample-containing vial through a hole in the cap septum. The fiber was positioned approximately 2 cm above the sample to collect volatile compounds (Figure 8). Sampling was typically conducted in a dark environment at room temperature for a duration of one day. Once sampling was complete, the fiber was retracted back into the needle to cease the collection process.

For gas chromatography (GC) analysis, the SPME needle, held by the SPME holder, was inserted into the sampling chamber through a SPME microseal equipped with a moulded Thermogreen LB-2 septa containing an injection hole. Inside the sampling chamber, the SPME needle was positioned in the SPME inlet liner. Once the fiber was released, the temperature in the sampling chamber was set to 250 °C to allow desorption of the compounds. The injection process was carried out in a splitless manner. The GC-MS analysis was performed by the Chemical, Molecular and Materials Analysis Centre (National University Singapore, Singapore) using an Agilent 7890A gas chromatograph coupled to an Agilent 5975C mass spectrometer (Agilent Technologies, Santa Clara, CA, USA). The chromatographic separation was achieved using a 30 m × 0.25 mm × 0.25 μM HP-5MS semipolar capillary column. The overall analysis time was 50 min. The oven temperature program started at 40 °C, then increased at a rate of 6 °C/min until reaching 80 °C. Subsequently, the temperature was increased at a rate of 3.4 °C/min until reaching 170 °C. Finally, the temperature was further increased at a rate of 12 °C/min until reaching a maximum of 300 °C, which was maintained for 4 min. The electron ionization potential was set to 70 eV, and the electron ionization (EI) source operated at a temperature of 230 °C. The quadrupole analyser was maintained at a temperature of 150 °C. Helium gas flowed through the column at a constant rate of 1.2 mL/min as the carrier gas. The mass spectrometer

detector operated in the positive polarity mode, scanning a mass range of 40-500 amu. The obtained EI mass spectra were compared to the NIST Mass Spectral Database for identification of the analytes.

Figure 8: SPME fibre assembly set-up for collection of sample analytes. A: *F. siamensis* sample with one cut plug with 1 g of autoclaved sieved soil; **B**: *F. siamensis* sample with six cut plugs; **C**: *R. microporus* sample with six cut plugs; **D**: PDA sample with six cut plugs. Scale bars are 10 mm.

2.2 Results

2.2.1 Volatile classification of air composition from various locations

Air samples from different locations were subjected to e-nose analysis to investigate the sensitivity of the e-nose sensors to changes in air composition across different environments. By using nitrogen as the baseline gas, the e-nose/CDA classification analysis was able to effectively differentiate air samples from various locations A to G, as indicated by the scatter plot CDA classification and the quantitative assessment of the data reading sets by the calculated MDist values exceeding 5.000 for each sample class (Figure 9). These findings demonstrate that air compositions vary across different locations, which can introduce an additional variable that may impact e-nose analysis if ambient air were to be used as the baseline gas.

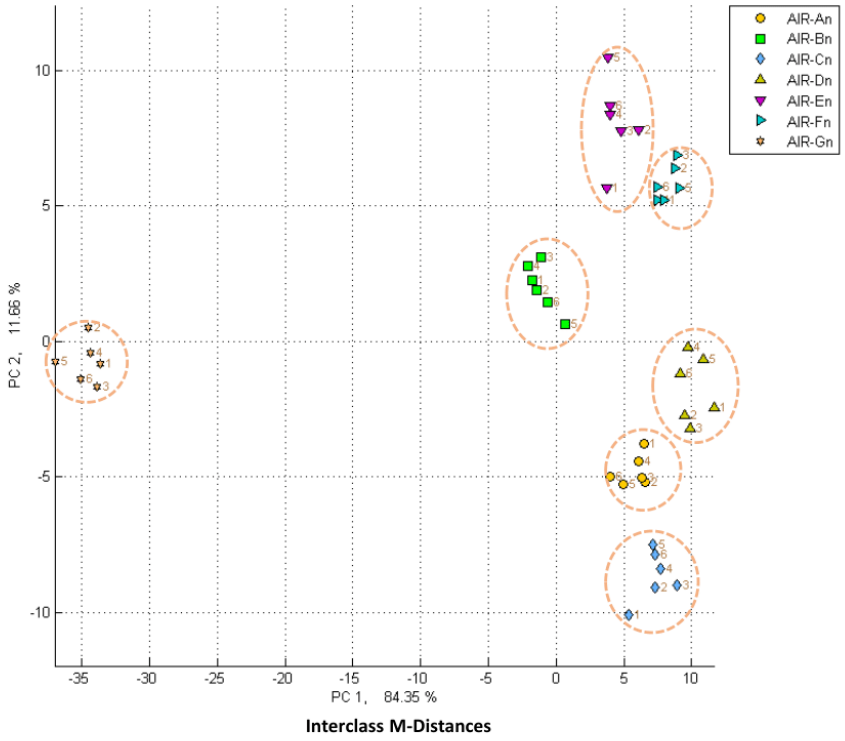

Interclass M-Distances

	AIR-An	AIR-Bn	AIR-Cn	AIR-Dn	AIR-En	AIR-Fn	AIR-Gn
AIR-An		10.634	5.605	6.764	13.572	11.991	40.829
AIR-Bn			14.886	14.096	10.001	13.369	34.481
AIR-Cn				8.135	17.211	15.166	42.820
AIR-Dn					11.745	9.224	44.957
AIR-En						7.825	40.263
AIR-Fn							43.689

Figure 9: Scatter plots with Canonical Discriminant Analysis (CDA) and calculated Interclass M-Distances (MDist) on e-nose volatile readings of air samples from different locations. Volatile classification by the e-nose of air samples at location A, B, C, D, E, F, G (AIR-An, AIR-Bn, AIR-Cn, AIR-Dn, AIR-En, AIR-Fn, AIR-Gn) with nitrogen as the baseline purge gas. Samples inside an orange dashed-line ellipse indicate that the MDist is greater than 5.000 and thus form a distinctive cluster. Data from Izzah Hazirah bte Junin [80].

2.2.2 E-nose methodology optimisation

Optimisation of the Cyranose 320 e-nose protocols was conducted through assessing its sensitivity and specificity to differentiate the selected plant and fungi-related VOCs under two different sensor purging conditions – using ambient air and using nitrogen gas. E-nose analysis when using the ambient air at location F (Table 2) as the baseline purge demonstrated that all VOCs, turpentine, farnesene and acetic acid, at concentrations of 5.0

ppm, 2.5 ppm, 0.5 ppm, and 0.25 ppm, could be qualitatively classified and differentiated from the air inside the biosafety cabinet (Table 2, location E) (labelled AIR-E). There was clear specificity with noticeable separations among the three volatiles turpentine (TUR0.25), farnesene (FAR0.25), and acetic acid (AA0.25) with concentration of 0.25 ppm, as indicated by MDist values exceeding 5.000 (Figure 10A). However, at a concentration of 0.05 ppm, only acetic acid (AA0.05) could still be distinctly clustered against the other VOCs. The remaining VOCs could not be clearly distinguished from each other, with MDist values of less than 5.000. The turpentine-farnesene (TUR0.05-FAR0.05) pairwise comparison exhibited the lowest MDist value of 2.649, indicating that the e-nose was unable to differentiate between their volatile profiles (Figure 10B).

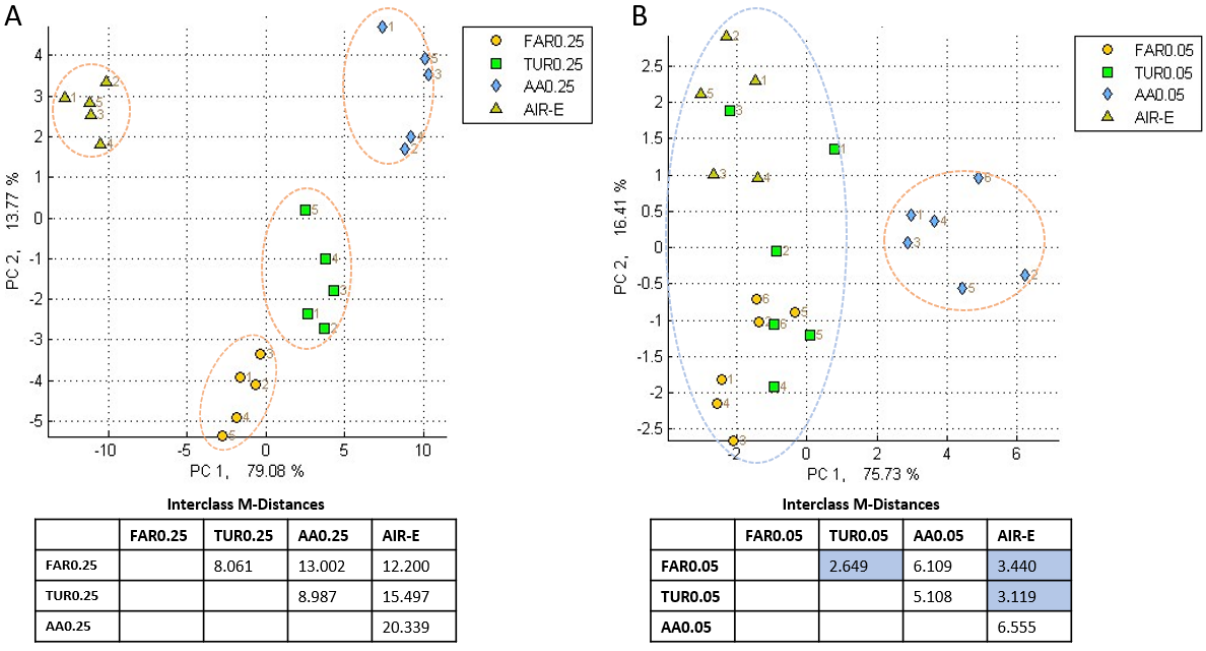

Interclass M-Distances

	FAR0.25	TUR0.25	AA0.25	AIR-E
FAR0.25		8.061	13.002	12.200
TUR0.25			8.987	15.497
AA0.25				20.339

Interclass M-Distances

	FAR0.05	TUR0.05	AA0.05	AIR-E
FAR0.05		2.649	6.109	3.440
TUR0.05			5.108	3.119
AA0.05				6.555

Figure 10: Scatter plots with Canonical Discriminant Analysis (CDA) and calculated Interclass M-Distances (MDist) on e-nose volatile readings of farnesene, turpentine, and acetic acid at low concentrations 0.25 ppm and 0.05 ppm with ambient air as baseline purge gas. A: Volatile classification by the e-nose of 0.25 ppm of farnesene (FAR0.25), turpentine (TUR0.25), acetic acid (AA0.25), and air from biosafety cabinet (AIR-E) volatile samples using ambient air as baseline gas; **B**: Volatile classification by the e-nose of 0.05 ppm volatile (FAR0.05, TUR0.05, AA0.05) samples using ambient air as the baseline gas. Samples inside an orange dashed-line ellipse indicate that the MDist is greater than 5.000 and thus form a distinctive cluster. Samples inside a blue dashed-line ellipse indicate a cluster of two samples with MDist less than 5.000, which is also indicated in blue in the pairwise comparison Interclass M-Distances table. Adapted from Tan et. al [81].

Using the same measurement parameters and same testing location (Table 2, location F), a pouch containing nitrogen gas was employed as the baseline purging gas for the e-nose. At a concentration of 0.25 ppm, the same VOCs exhibited distinct clustering with higher MDist values, indicating improved specificity (Figure 11A). When analysing VOCs at 0.05 ppm, the e-nose using nitrogen as the baseline gas was able to clearly differentiate the air (AIR-En), turpentine (TUR0.05n), farnesene (FAR0.05n), and acetic acid (AA0.05n) volatiles from each other, with pairwise MDist values exceeding 5.000 for each comparison (Figure 11B). Notably, the turpentine-farnesene (TUR0.05n-FAR0.05n) pairwise comparison demonstrated a substantial enhancement, with an MDist value of 9.967, compared to the use of ambient air as the baseline gas (MDist value 2.649).

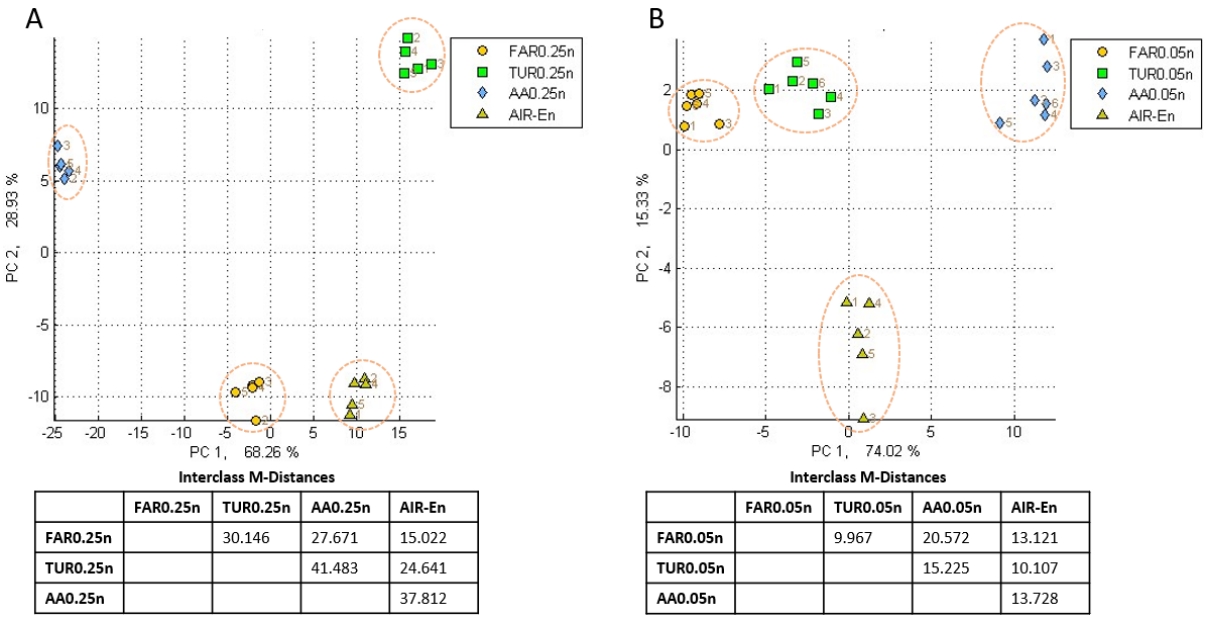

Interclass M-Distances

	FAR0.25n	TUR0.25n	AA0.25n	AIR-En
FAR0.25n		30.146	27.671	15.022
TUR0.25n			41.483	24.641
AA0.25n				37.812

Interclass M-Distances

	FAR0.05n	TUR0.05n	AA0.05n	AIR-En
FAR0.05n		9.967	20.572	13.121
TUR0.05n			15.225	10.107
AA0.05n				13.728

Figure 11: Scatter plots with Canonical Discriminant Analysis (CDA) and calculated Interclass M-Distances (MDist) on e-nose volatile readings of farnesene, turpentine, and acetic acid at low concentrations 0.25 ppm and 0.05 ppm with nitrogen as baseline purge gas. A: Volatile classification by the e-nose of 0.25 ppm of farnesene (FAR0.25n), turpentine (TUR0.25n), acetic acid (AA0.25n), and air from biosafety cabinet (AIR-En) volatile samples using nitrogen as the baseline gas; **B**: Volatile classification by the e-nose of 0.05 ppm volatile (FAR0.05n, TUR0.05n, AA0.05n) samples using nitrogen as the baseline gas. Samples inside an orange dashed-line ellipse indicate that the MDist is greater than 5.000 and thus form a distinctive cluster. Adapted from Tan et. al [81].

By conducting statistical analysis on the resistance change data ($\Delta R/R_o$) from the 32 sensors using nitrogen as the baseline gas, sensors 6, 23, 24, 31, and 32 were the primary active sensors, accounting for the highest variance (8.151%, 6.894%, 6.881%, 37.407%, and 36.937% respectively) across the sample readings (Figure 12A). Sensors 23 and 24 exhibited negative responses, indicating an increase in resistance when exposed to farnesene, turpentine and air samples, which enhances the e-nose's resolution when using nitrogen as the baseline gas.

In contrast, when ambient air was used as the baseline gas, only sensors 31 and 32 (48.608% and 47.957% respectively) were identified as active sensors, contributing the most to the variance in the sample readings, while sensors 6, 23, and 24 made negligible contributions (Figure 12B). This shows that the use of nitrogen as the baseline gas activates a greater number of sensors. Furthermore, it was observed that the magnitude of response for the same responsive sensors (31 and 32) was significantly increased when using nitrogen as the baseline gas compared to ambient air. This increase in response magnitude could have accounted for the improved sensitivity and higher discriminant ability of the e-nose.

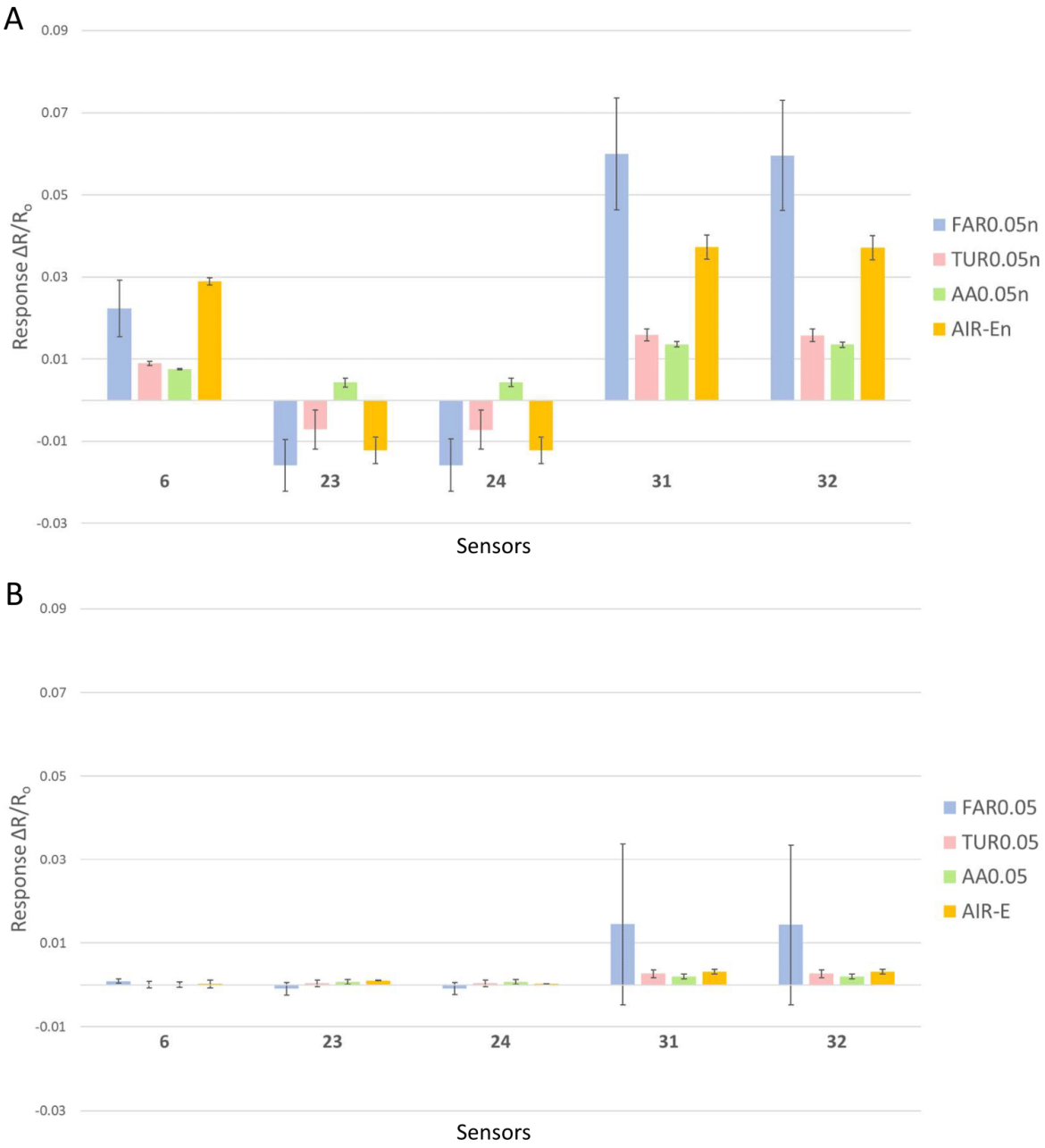

Figure 12: Average resistance data response ($\Delta R/R_o$) of the selected active sensors. A: Resistance readings of the e-nose from 0.05 ppm of samples farnesene (FAR0.05n), turpentine (TUR0.05n), acetic acid (AA0.05n) and air from biosafety cabinet (AIR-En) when using nitrogen the baseline gas; **B**: Resistance readings of the e-nose from 0.05 ppm of samples farnesene (FAR0.05), turpentine (TUR0.05), acetic acid (AA0.05) and air from biosafety cabinet (AIR-E) when using ambient air as the baseline gas. Adapted from Tan et. al [81].

Comparison of the use of ambient air with the new protocol using nitrogen gas was also conducted on purified fungal mycelia cut plug samples (Table 3) of *Fulvifomes siamensis*, *Rigidoporus microporus*, and *Pyrrhoderma noxium*. The number of Principal Components

(PCs) for dimensional reduction during Canonical Discriminant Analysis (CDA) was also varied to observe how an increase in PCs could affect the classification outcome of the results.

The larger MDist values when using nitrogen gas as compared to ambient air demonstrates that the new protocol using nitrogen gas greatly increased the sensitivity of the e-nose to the different species of wood rot fungi (Figure 13). When ambient air was used as the baseline gas and under four PCs for dimension reduction, the e-nose was unable to distinguish between the *R. microporus* samples from the *P. noxium* samples, with an MDist of 2.969 (Figure 13A). Whereas when nitrogen gas was used as the baseline gas and under four PCs for dimension reduction, the e-nose could successfully differentiate between all three fungi species with MDist above 5.000 (Figure 13C).

The increase of PCs for dimensional reduction was also demonstrated to improve the species-specific classification by the CDA algorithm. When ten PCs were used for dimension reduction, the classification of the readings taken with the ambient air protocol could then be differentiated by species with MDist above 5.000 (Figure 13B). Moreover, with the new protocol with nitrogen gas and at ten PCs for dimension reduction, the MDist values greatly increased, indicating that the volatile profiles of the different species were more clearly distinguished from each other. Hence, not only does the nitrogen gas baseline purge improve the species-specific volatile profiling by the e-nose, the choice of PCs selected for dimensional reduction is also crucial for results analysis, of which this thesis chose a minimum of ten PCs as the default for subsequent analysis.

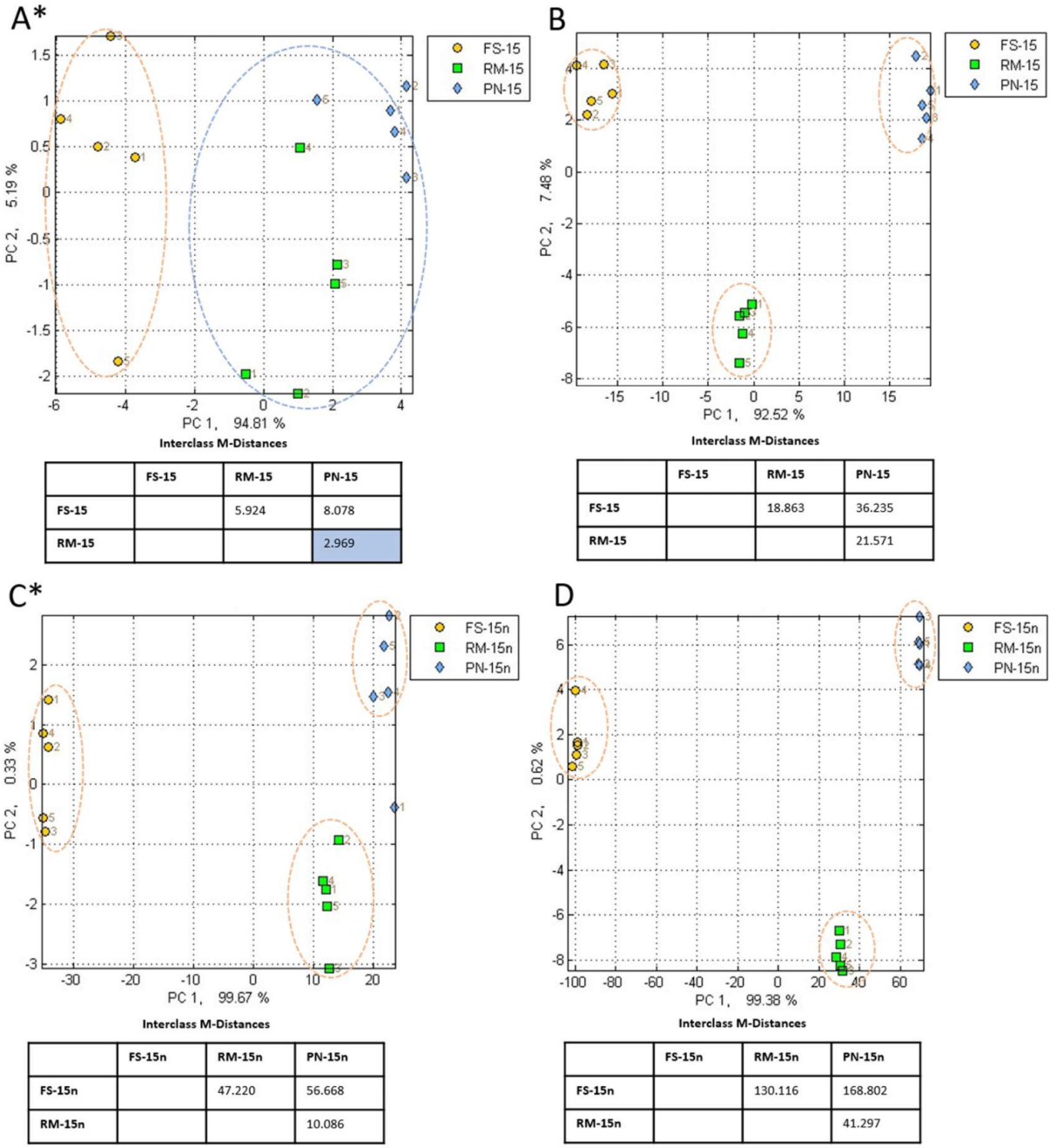

	FS-15	RM-15	PN-15
FS-15		5.924	8.078
RM-15			2.969

	FS-15	RM-15	PN-15
FS-15		18.863	36.235
RM-15			21.571

	FS-15n	RM-15n	PN-15n
FS-15n		47.220	56.668
RM-15n			10.086

	FS-15n	RM-15n	PN-15n
FS-15n		130.116	168.802
RM-15n			41.297

Figure 13: Scatter plots with Canonical Discriminant Analysis (CDA) and calculated Interclass M-Distances (MDist) on e-nose volatile readings of fungal mycelia under two different sensor purging conditions. Volatile classification by the e-nose of 15 cut plugs of *F. siamensis* (FS-15), *R. microporus* (RM-15), *P. noxium* (PN-15) using ambient air as baseline purge with **A**: 4 PCs used for canonical graph, **B**: 10 PCs used for canonical graph; Volatile classification by the e-nose of 15 cut plugs of *F. siamensis* (FS-15n), *R. microporus* (RM-15n), *P. noxium* (PN-15n) using nitrogen gas as baseline purge with **C**: 4 PCs used for canonical graph; **D**: 10 PCs used for canonical graph. Samples inside an orange dashed-line ellipse indicate that the MDist is greater than 5.000 and thus form a distinctive cluster. Samples inside a blue dashed-line ellipse indicates a cluster of two samples with MDist less than 5.000, which is also indicated in blue in the pairwise comparison table. * indicates that the number of PCs used for the canonical graph was 4 instead of 10 (default).

2.2.3 Volatile analysis of fungi mycelia cut plugs from various species

The e-nose with nitrogen as the baseline gas and downstream use of CDA with ten PCs was utilized to classify the volatile profiles of pure fungi culture cut plugs of the six pathogenic fungi *F. siamensis*, *R. microporus*, *L. theobromae*, *P. noxium*, *G. orbiforme* and *G. australe*, from PDA media with no fungus growth (AGAR) (Figure 14). CDA results showed distinct classification of the fifteen fungal mycelia cut plugs of all six species and the control sample (AGAR) within 15 min of sample incubation. The high MDist value of larger than 10.000 for all pairwise comparison gives strong confidence of the sensitivity and specificity of the e-nose to distinguish fungal mycelia volatiles with minimal mycelia sample (around 55 mg fresh weight).

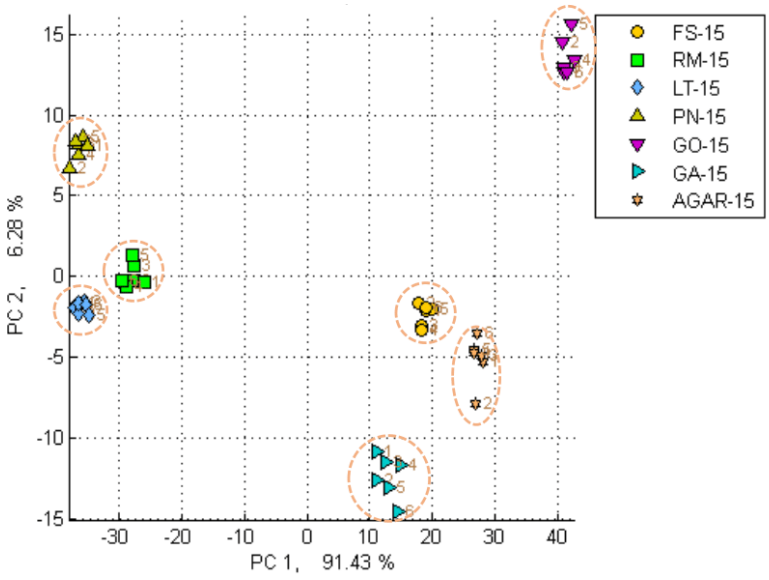

Interclass M-Distances

	FS-15	RM-15	LT-15	PN-15	GO-15	GA-15	AGAR-15
FS-15		47.195	55.802	56.294	29.925	16.564	12.937
RM-15			10.596	11.965	70.676	42.908	55.574
LT-15				12.176	78.896	50.282	63.358
PN-15					78.103	53.576	65.045
GO-15						38.669	24.465
GA-15							18.448

Figure 14: Scatter plots with Canonical Discriminant Analysis (CDA) and calculated Interclass M-Distances (MDist) on e-nose volatile readings of six fungi mycelia strains. Volatile classification by the e-nose of fifteen cut plugs of *F. siamensis* (FS-15), *R.* microporus (RM-15), *L .theobromae* (LT-15), *P. noxium* (PN-15), *G. orbiforme* (GO-15), *G. australe* (GA-15) samples using nitrogen as the baseline gas. Samples inside an orange dashed-line ellipse indicate that the MDist is greater than 5.000 and thus form a distinctive cluster.

While the e-nose/CDA tool can be used to classify volatile profiles of the wood rot samples, it is unable to quantify and identify the volatiles of these samples. Hence, SPME-GC-MS was utilised to verify the distinct differences of the volatile profiles between the different fungi species. SPME-GC-MS identifies the composition of volatiles by the retention time from the gas chromatogram and comparing the mass spectrum from mass spectrometry to a database of known mass spectra. The relative abundance for each volatile analyte can also be computed through dividing the volatile's peak area by the total area of all detected peaks. In this thesis, the name of each compositional volatile with good quality reading (above 90), its Chemical Abstracts Service (CAS) unique identification number, and the relative abundance of each peak (represented by the number of asterisks) are presented in a table.

Volatiles of four selected fungi mycelia cut plugs, *L. theobromae, R. microporus, F. siamensis* and *P. noxium*, were tested using the SPME-GC-MS analysis (Table 4). Unique volatiles that were only present in a species-specific manner, and with high abundance (greater than 5% abundance), were identified for three of the pathogen fungi mycelia cut plugs, namely: 5,6-dihydro-6-propyl-2H-pyran-2-one for *L. theobromae*; cetrimonium bromide, methyl ester benzoic acid and tributylamine for *R. microporus*; 1,2,4,5-tetrachloro-3,6-dimethoxybenzene and beta-farnesene for *F. siamensis*. The data provided further evidence in support of how different fungi emit unique profiles of VOCs which could have allowed to e-nose/CDA tool to distinctly classify the volatile profiles.

Table 4: Volatiles of selected culture samples identified by SPME-GC-MS

Volatile	CAS No.	*Agar**	*LT* Culture*	*PN* Culture*	*RM* Culture*	*FS* Culture*	*FS* Soil*
2-(1,3-Benzodioxol-5-ylmethyl)-1H-isoindole-1,3(2H)-dione	997493-03-6				**		
2,2,4-Trimethyl-1,3-pentanediol diisobutyrate	006846-50-0			**	**		
2,4-Di-tert-butylphenol	000096-76-4		**	**		*	
2,5-Cyclohexadiene-1,4-dione, 2,6-bis(1,1-dimethylethyl)-	000719-22-2		**				**
2,6-Diisopropylnaphthalene	024157-81-1	**					
2,7-dichloro-1-methoxydibenzofuran	067061-60-3					**	
2-Benzylidenehydrazono-3-methyl-2,3-dihydrobenzothiazole	997443-22-4			**			
2H-Pyran-2-one, 5,6-dihydro-6-propyl-	016400-69-4		***				
2-Propenoic acid, 2-ethylhexyl ester	000103-11-7	**					
3-Octanone	000106-68-3			***		*	
4-Isopropyl-1,6-dimethyl-1,2,3,4-tetrahydronaphthalene	000483-77-2	**	**				
9-Octadecenoic acid (Z)-, methyl ester	000112-62-9						**
9-Octadecenoic acid, (E)-	000112-79-8						**
Acetic acid, 2-phenylethyl ester	000103-45-7					**	
alpha-Muurolene	031983-22-9			**		*	
Aristolochene	026620-71-3		**				
Benzaldehyde	000100-52-7			**			
Benzene, 1-(1,5-dimethyl-4-hexenyl)-4-methyl	000644-30-4					*	***
Benzene, 1,2,4,5-tetrachloro-3,6-dimethoxy-	000944-78-5					*****	*
Benzene, 1,4-dichloro-2,5-dimethoxy-	002675-77-6					*	
Benzoic acid, methyl ester	000093-58-3				***		
beta-Farnesene	018794-84-8					*****	
Cetrimonium Bromide	000057-09-0				*****		
Dedecane, 1-iodo	004292-19-7		**				
Dimethyl palmitamine	000112-69-6						***
Docosane	000629-97-0		**				**
Hexadecane, 1-chloro-	004860-03-1				**		
Methyl 2,6-Dichloro-4-methoxybenzoate	094278-65-6					**	
Methylbenzoate	000093-58-3			**			
Octadecane	000593-45-3						**
trans-Calamenene	073209-42-4			**			
Tributylamine	000102-82-9				***		
Undecanone	000112-12-9			*			

Legend	
Relative abundance	
	< 0.1%
*	0.1–1%
**	1–5%
***	5–10%
*****	> 20%

*Abbreviations: Agar for PDA cut plug sample; LT for *L. theobromae;* PN for *P. noxium*; RM for *R. microporus*; FS for *F. siamensis*; FS soil for *F. siamensis* cut plug sample mixed with soil.

Apart from testing pure fungal mycelia cultures, the volatile profiles of the mycelia cut plugs mixed with garden soil was also analysed. SPME-GC-MS conducted on a *F. siamensis* cut plug sample mixed with soil revealed that key volatile of FS 1,2,4,5-tetrachloro-3,6-dimethoxybenzene significantly reduced from 23.63% (*****) to 0.51% (*) while volatiles such as 9-octadecenoic acid (abundance 5.0%), dimethyl palmitamine (abundance 8.76%) and octadecane (abundance 1.53%) that were initially not present in the pure mycelia sample, were in higher amounts after mixture with soil (Table 4).

At ten Principal Components (PCs) dimension reduction, clustering results reveal that the 3 strains of fungi cut plug mixed with soil could be well-differentiated from the control samples (SOIL and AGAR-10-S) without pathogenic fungi (Figure 15). However, the *F. siamensis* (FS-10-S1, FS-10-S2), *R. microporus* (RM-10-S1, RM-10-S2) and *P. noxium* (PN-10-S1, PN-10-S2) samples were not clearly distinguishable from each other after the addition of soil even when 32 PCs were used for dimension reduction (data not shown).

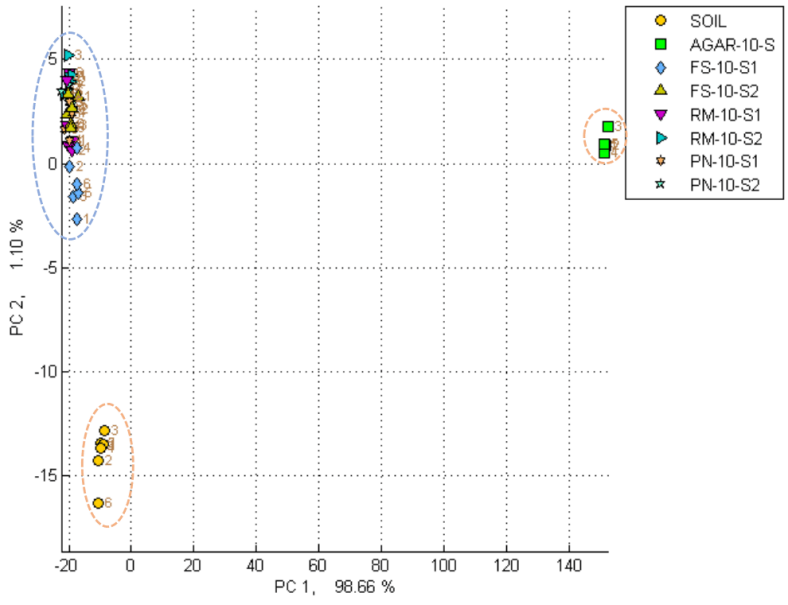

Interclass M-Distances

	SOIL	AGAR-10-S	FS-10-S1	FS-10-S2	RM-10-S1	RM-10-S2	PN-10-S1	PN-10-S2
SOIL		162.128	16.738	19.561	19.075	20.876	19.473	19.636
AGAR-10-S			169.756	171.104	171.589	171.739	171.836	171.234
FS-10-S1				4.652	8.092	9.633	6.625	8.178
FS-10-S2					4.606	5.515	2.715	4.330
RM-10-S1						2.110	1.991	0.985
RM-10-S2							3.160	1.535
PN-10-S1								1.908

Figure 15: Scatter plots with Canonical Discriminant Analysis (CDA) and calculated Interclass M-Distances (MDist) on e-nose volatile readings of fungi mycelia strains with soil. Volatile classification by the e-nose of soil mixed with ten cut plugs of *F. siamensis* duplicate samples (FS-10-S1, FS-10-S2), *R.* microporus duplicate samples (RM-10-S1, RM-10-S2), *P. noxium* duplicate samples (PN-10-S1, PN-10-S2) against soil mixed with PDA media cut plugs (AGAR-10-S) and pure soil (SOIL) samples using nitrogen as the baseline gas. Samples inside an orange dashed-line ellipse indicate that the MDist is greater than 5.000 and thus form a distinctive cluster. Samples inside a blue dashed-line ellipse indicate a cluster of two samples with MDist less than 5.000, which is also indicated in blue in the pairwise comparison Interclass M-Distances table.

2.2.4 Volatile profile classification based on concentration

By utilizing the CDA algorithm with ten PCs and employing nitrogen as the baseline gas, the analysis of single volatiles at different concentrations (0.05, 0.25, 0.5, 2.5, and 5 ppm) exhibited quantitative-based clustering, although the resolution of clustering varied among the different VOCs. The clustering of acetic acid at the five varying concentrations (Figure 16A) resulted in distinct classes corresponding to the respective concentrations. In contrast, the turpentine samples were divided into four classes (Figure 16B), with the samples of 0.05 ppm (TUR0.05n) and 0.25 ppm (TUR0.25n) clustered together.

Similarly, the e-nose with nitrogen as the baseline gas was able to detect the quantitative change and differentiate varying numbers of fungi mycelia cut plugs (five, ten, and fifteen) of *F. siamensis*, *R. microporus*, *P. noxium*, *L. theobromae*, and *G. orbiforme*. For *G. australe* samples, the e-nose was only able to discriminate the fifteen cut plugs from the rest, while the pairwise comparison of five-ten cut plugs were clustered together (Appendix A).

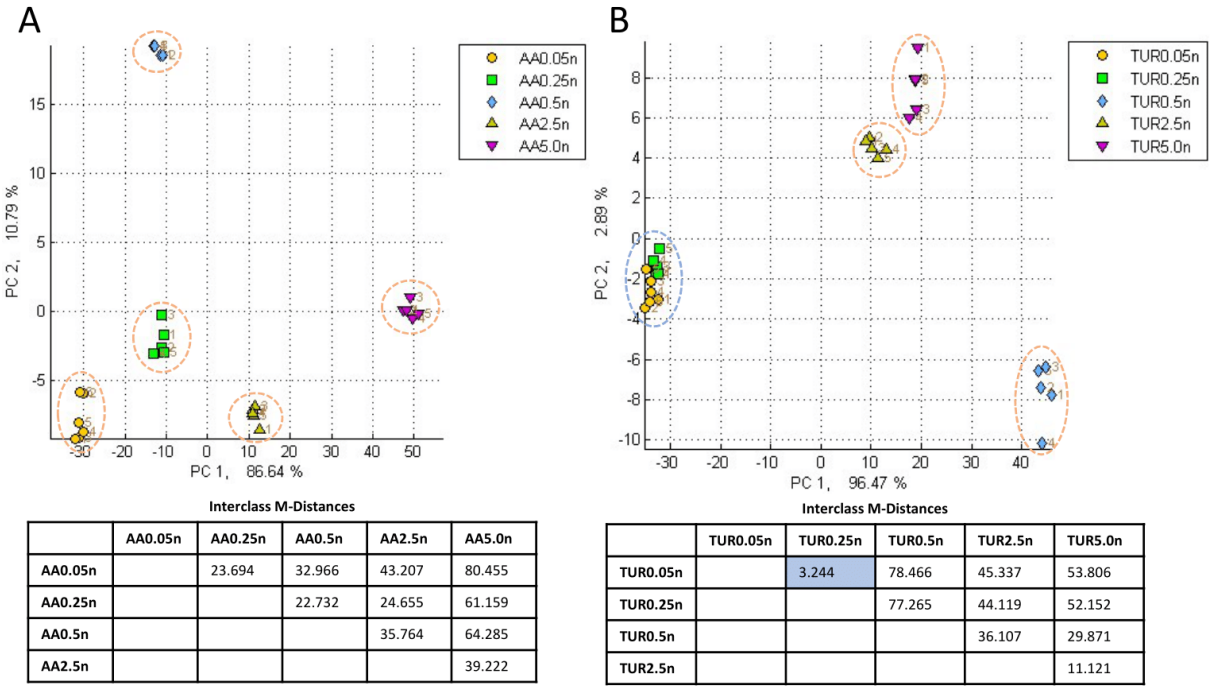

Interclass M-Distances

	AA0.05n	AA0.25n	AA0.5n	AA2.5n	AA5.0n
AA0.05n		23.694	32.966	43.207	80.455
AA0.25n			22.732	24.655	61.159
AA0.5n				35.764	64.285
AA2.5n					39.222

Interclass M-Distances

	TUR0.05n	TUR0.25n	TUR0.5n	TUR2.5n	TUR5.0n
TUR0.05n		3.244	78.466	45.337	53.806
TUR0.25n			77.265	44.119	52.152
TUR0.5n				36.107	29.871
TUR2.5n					11.121

Figure 16: Scatter plots with Canonical Discriminant Analysis (CDA) and calculated Interclass M-Distances (MDist) on e-nose volatile readings of acetic acid and turpentine at varying concentrations. A:Volatile classification by the e-nose of varying concentrations 0.05, 0.25, 0.5, 2.5 and 5.0 ppm acetic acid (AA0.05n, AA0.25n, AA0.5n, AA2.5n, AA5.0n); and **B**: turpentine (TUR0.05n, TUR0.25n, TUR0.5n, TUR2.5n, TUR5.0n) using nitrogen as the baseline gas. Samples inside an orange dashed-line ellipse indicate that the MDist is greater than 5.000 and thus form a distinctive cluster. Samples inside a blue dashed-line ellipse indicates a cluster of two samples with MDist less than 5.000, which is also indicated in blue in the pairwise comparison Interclass M-Distances table. Adapted from Tan et. al [81].

2.3 Discussion

This chapter, specifically subsection 2.2.1 and 2.2.2, displayed the importance of using nitrogen gas as the baseline purge gas for the e-nose sensors as an improved protocol for e-nose volatile analysis. It is crucial to establish a consistent baseline gas (R_o) because VOCs are classified based on the $\Delta R/R_o$ data measured across the sensor array of the Cyranose 320.

Although using ambient air is convenient, it does not provide consistent results as the composition of ambient air can vary depending on the surrounding environment (Figure 9). These variations could arise from factors like automobile emissions or industrial waste volatiles, which could influence the performance of the e-nose when deployed in field applications near roadsides or industrial parks. When ambient air is used as the baseline gas for the e-nose, the remaining air in the chamber may contain pollutants such as sulfur dioxide, nitrogen dioxide and carbon monoxide [82] which could react differently with the various volatiles from the samples, thereby influencing sensor responses. The inconsistent composition of air introduces variability that diminishes the discriminant capability of the e-nose.

The use of nitrogen gas for the e-nose could mitigate potential variations caused by different ambient air compositions in various operational environments. Nitrogen gas is also commonly used in industrial applications as a zero gas or purging gas [83]. Through tests using selected plant and fungi-related volatiles and employing nitrogen as the baseline gas, the sensitivity and specificity of e-nose detection significantly improved. This improvement was evident through distinct clustering even at lower concentrations of sample analyte at 0.05 ppm. When ambient air served as the baseline gas, the e-nose was unable to distinguish between turpentine and farnesene (Figure 10B). This could possibly be due to their closely related chemical structures which react to the sensors similarly as they both belong to the overarching class of terpenoids. In contrast, when nitrogen was used as the baseline gas, the e-nose was able to clearly differentiate all volatiles, turpentine, farnesene and acetic acid from the air sample at a concentration of 0.05 ppm (Figure 11B), showing that there was an increased sensitivity towards the different volatiles despite having similar characteristics. This increased sensitivity with nitrogen gas would be useful especially to distinguish volatiles

evolved from wood rot pathogenesis which could consist of chemicals of similar structure and from the same class such as terpenoids and benzenoids [56,84-86].

Subsequent examination of sensor responses revealed an increased number of sensors exhibiting responsiveness when nitrogen was employed as the baseline gas, potentially leading to an enhancement in clustering resolution. Additionally, when comparing the same responsive sensors under both nitrogen and ambient air as the baseline gas, the magnitude of response was significantly higher when nitrogen was utilized (Figure 12). This enhancement can be attributed to the inert properties of nitrogen gas. By displacing oxygen and other pro-oxidative gases, nitrogen effectively purges impurities from the sensors during baseline gas recording. These findings show that the greater number of responsive sensors and the higher magnitude of their responses are key factors contributing to the improved sensitivity. Therefore, employing nitrogen as the baseline gas is more appropriate as it not only mitigates the impact of additional variables ambient air has on e-nose readings, but also improve sensor sensitivity to the samples' analytes.

Furthermore, when tested with fungal mycelia cut plugs, the e-nose/nitrogen protocol (Figure 13C, 13D) fared better than the e-nose/ambient air protocol (Figure 13A, 13B) in distinguishing the volatile profiles of three fungi species after post-data classification analysis with higher MDist values for every pairwise comparison. The choice of the number of Principal Components (PCs) was also highlighted in the results, which showed how an increase in the number of PCs from four PCs to ten PCs during dimension reduction could improve the distinction and classification of the volatile profiles. This is especially seen in the improvement of classification under the ambient air protocol whereby all three fungi species could be clearly differentiated under the ten PCs dimension reduction (Figure 13B), whereas *R. microporus* and *P. noxium* samples could not be differentiated under the four PCs dimension reduction (Figure 13A). A higher number of PCs would mean that data from more

sensors (i.e. from four sensors to ten sensors) were considered for the plotting of volatile profile data on the canonical plots, which thereby allows the visualisation of more differences between each sample.

Nonetheless, there needs to be consideration to choose a low number of PCs for dimension reduction as a large number of sensors may include unnecessary noise and distinction between samples. For instance, in reference to Figure 12, three sensors (sensors 6, 23, 24) under the ambient air protocol, displayed low sensitivity and the resistance change profile behaves very differently in comparison to the nitrogen protocol. Hence, a higher number of sensors chosen will not necessarily help to improve volatile profile classification in the case of the ambient air protocol. As for the nitrogen protocol, data introduced by more than ten sensors may separate data points further and appear to be a separate class or species. Thus, more sensors may be a noise due to the increased sensitivity.

Using the optimised protocol of nitrogen as the baseline gas, the e-nose/CDA tool was able to effectively differentiate between the volatile profiles of all six species of fungal mycelia cut plugs *F. siamensis, R. microporus, P. noxium, L. theobromae, G. orbiforme* and *G. australe* (Figure 14). These unique profiles were substantiated by GC-MS results conducted on selected fungi mycelia cut plug samples for the first four species (Table 4).

Some fungi species had unique volatiles that make up more than 5% total abundance. *L. theobromae* had 5,6-dihydro-6-propyl-2H-pyran-2-one ($C_8H_{12}O_2$) released as a unique volatile that the other sampled fungi mycelia did not have. This volatile has been identified in the fermentation products of *Cordyceps sinensis* mycelia, another fungi belonging to the Ascomycota phylum [87]. With a similar criterion of more than 5% total abundance, *R. microporus* had two specific volatiles – cetrimonium bromide ($C_{19}H_{42}BrN$), and methyl ester benzoic acid ($C_8H_8O_2$). Cetrimonium bromide is a quaternary ammonium surfactant that is

known to be antiseptic against bacteria and fungi [88], it is also commonly used in DNA extraction methods for archaea, bacteria, fungi, and plant materials with high polysaccharide contents [89]. Biosynthesis of methyl esters benzoic acid (and other aromatic acids) occur commonly during primary metabolism of fungi such as *Phellinus pomaceus* [90], a fungi belonging to Agaricomycetes similar to *R. microporus*. While tributylamine ($C_{12}H_{27}N$) was also present in the *R. microporus* sample in a high abundance (5-10%), it is an ion-pairing reagent which is commonly used in metabolite studies as part of the solvent in liquid chromatography-mass spectrometry [91-93]. *F. siamensis* had two volatiles in high abundance, namely 1,2,4,5-tetrachloro-3,6-dimethoxybenzene ($C_8H_6Cl_4O_2$) and beta-farnesene ($C_{15}H_{24}$), both with abundance of more than 20%. 1,2,4,5-tetrachloro-3,6-dimethoxybenzene has been identified to be a natural product found in *Agaricus bisporus*, belonging to the same class as *F. siamensis* – Agaricomycetes [94]. Furthermore, it is an analogue to tetrachloro-1,4-dimethoxybenzene which is a well-studied as a secondary metabolite of fungi from the subkingdom Basidiomycota [94]. Overall, these results demonstrate the unique volatile portfolios of the pure fungal mycelia, of which the e-nose downstream classification analysis has shown successful species-specific differentiation that could be useful in the field application in detecting presence of these wood rot fungi.

Further investigation of the e-nose's performance in detecting fungal mycelia cut plugs in soil resulted in a significant reduction in the specificity of classification between *F. siamensis, R. microporus* and *P. noxium* samples. While the e-nose could still differentiate the control PDA media cut plug sample from the fungal mycelia cut plug samples upon mixture with garden soil, the fungal mycelia samples were clustered together (Figure 15). This outcome demonstrates that the volatiles from the soil might have diluted, or the soil may have preferentially absorbed some of the pathogen-specific volatiles during e-nose testing, resulting in poor resolution between the pathogen samples. Through the SPME-GC-MS

analysis of the *F. siamensis* mycelia cut plug sample mixed with soil (Table 4), the volatile 1,2,4,5-tetrachloro-3,6-dimethoxybenzene significantly decreased in the total volatile abundance from more than 20% in the mycelia cut plug sample alone, to around 0.51% when mixed with soil. Instead, volatiles such as 9-octadecenoic acid ($C_{18}H_{34}O$) and dimethyl palmitamine ($C_{18}H_{39}N$) which are natural products of plants could have been contributed from plant materials that have integrated together with the garden soil [95,96]. Consequently, soil sampling may not be the ideal method for the pathogen-specific field diagnosis using the Cyranose 320 e-nose due to potential soil particle volatile contribution that dilutes the disease-related volatiles. Hence, application to the field diagnosis tests with volatile-based tools should consider the use of tree tissue material and fungi basidiocarps instead.

Apart from differentiating based on fungal species, volatile concentration, which may be affected based on the amount of mycelia present, can influence the e-nose clustering of the samples. Although the usage of the 'Normalisation 1' tool (methodology subsection 2.1.2) was utilised during data processing to reduce the effect of volatile quantity on the canonical clustering results, results show that the concentration of volatiles could still influence the sample classification (Figure 16). Therefore, the presence of a variable response dependent on volatile quantity adds complexity to the e-nose diagnosis, which was initially expected to be focused on the classification based on chemical structure. This observation indicates the potential for quantitative analysis using the Cyranose 320 e-nose, which has not been previously reported. This feature could be further explored to determine the infection progression, given that the amount of fungal pathogen would increase over time, which could be then led to a greater expected concentration of specific target volatile compounds.

Chapter 3: Field application of volatile-based diagnosis for wood rot disease

While Chapter 2 focuses on the concept-proof of the unique volatile emissions by pure strains of wood rot fungi grown on culture media and e-nose technical improvements, this chapter explores the application of the volatile-based diagnosis techniques on samples that involve host tree-fungi interactions – the early stage incipient infection of wood rot fungi in wood tissues; and late stage disease development of fruiting bodies on host trees.

This thesis serves as a continuation of the *in vitro* wood decay study done by Hong et al. [13] which assessed the extent of wood decay in wood blocks obtained from tree branches after treatment with *F. siamensis, R. microporus* and *P. noxium* for 12 weeks. This *in vitro* study would simulate early stage infections of wood rot in host trees. In subsection 3.2.1, four species of host trees wood blocks (Angsana, Casuarina, Khaya, Rain tree) were inoculated with *F. siamensis* and *R. microporus* under varying incubation time (two, four, six and eight weeks). Their volatile profiles were then analysed. *F. siamensis* was selected because it was the most widely present in tree species, and in particular Angsana, Casuarina, Khaya and Rain tree that were significantly susceptible to damage by the fungus. Hence these four trees were selected during this investigation. *R. microporus* was selected as a second species and was chosen over *P. noxium* as *R. microporus* was found to cause a more significant loss in dry wood weight of Khaya and Rain tree wood blocks [13]. This work was done in collaboration with a Final Year Project of Izzah Hazirah bte Junin [80].

Field application of the e-nose was then assessed on its ability to distinguish volatile profiles of wood rot late stage disease samples such as wood tissues and basidiocarps from *F. siamensis, R. microporus, P. noxium, G. orbiforme* and *G. australe.* A prior Final Year Project study done by Zhang Ziteng [97] established that a short incubation time for samples in the bag was necessary and sufficient for volatile equilibration prior to e-nose analysis. This

chapter adopted a 15 min sample incubation time for the field samples prior to the e-nose diagnosis and identification testing with nitrogen gas as the baseline. This thesis utilised many samples of *F. siamensis* to generate sufficient training data and created a model that demonstrated successful real-time field application of species-specific identification of samples affected by *F. siamensis*.

3.1 Methodology

In this section, we outline the methodology for conducting an *in vitro* pathogenesis study of two wood rot fungi on wood blocks from four different tree species, as detailed in subsection 3.1.1. Following this, subsection 3.1.2 focuses on the statistical analysis of the changes in wood block weights after fungal incubation, offering insights into the extent of fungal decay. Subsection 3.1.3 describes the approach to volatile-based testing on these wood blocks, employing the e-nose and SPME-GC-MS after exposure to the wood rot fungi, providing a comprehensive overview of the volatile compounds emitted during the decay process.

Subsection 3.1.4 details the collection and analysis of late stage wood rot disease tissues and basidiocarps. This includes details on the sample processing, DNA extraction, barcoding, and the volatile analysis using the e-nose and SPME-GC-MS. Finally, subsection 3.1.5 delves into the development of a predictive model and the usage of the e-nose technology for real-time diagnosis of wood rot diseases.

3.1.1 In vitro pathogenesis study of wood rot fungi on wood blocks

Branches from four tree species that are commonly planted in Singapore [13], Angsana, Casuarina, Khaya and Rain tree were obtained from the National Parks Board of Singapore (NParks). The methodology from Hong et al. [13] was adapted for this *in vitro* study of ‘diseased wood blocks’ using the e-nose and SPME-GC-MS.

Wood blocks measuring 30 mm x 10 mm x 8 mm were cut from the branches and dried at 100 ˚C for 48 h in an Incucell 55 incubator (MMM Group, Planegg, Germany). Their dry weights were then measured with a precision balance (BEL Engineering, Monza, Italy). Wood blocks were labelled according to the tree species, 'A' for Angsana wood blocks, 'C' for Casuarina wood blocks, 'K' for Khaya wood blocks and 'R' for Rain tree wood blocks, followed by the treatment type (i.e. FS for *F. siamensis*, RM for *R. microporus*, CN for control), and ends with the incubation period (i.e. 2w, 4w, 6w, 8w for two, four, six, and eight weeks of incubation respectively). For instance, sample C-FS-2w represents Casuarina wood block sample incubated in *F. siamensis* culture for 2 weeks. Prior to the treatment of the wood blocks on the culture plates, they were autoclaved twice at 121˚C for 30 min.

Fungal culture preparation and DNA isolation was conducted (subsection 2.1.6) for the selected key pathogen cultures of *F. siamensis* and *R. microporus* for wood block treatment. The pure fungal isolates were grown on 2.4% PDA media without antibiotics culture plates (90 mm diameter) (Biomedia, Singapore) incubated at 25˚C for 14 days to allow the fungal mycelia growth to cover the entire plate.

Two autoclaved wood blocks from the same species were placed on the test fungus cultured plates (Figure 17A, 17B). For a control reference group, two autoclaved wood blocks from the same species were placed onto 2.4% PDA media plates that do not contain fungal culture (Figure 17C). The plates were sealed and incubated at 25 ˚C for varying incubation period of two, four, six and eight weeks. This process was repeated for all four tree species. Each fungus species and tree species wood block combination had three replicate plates (triplicates) for each incubation period time.

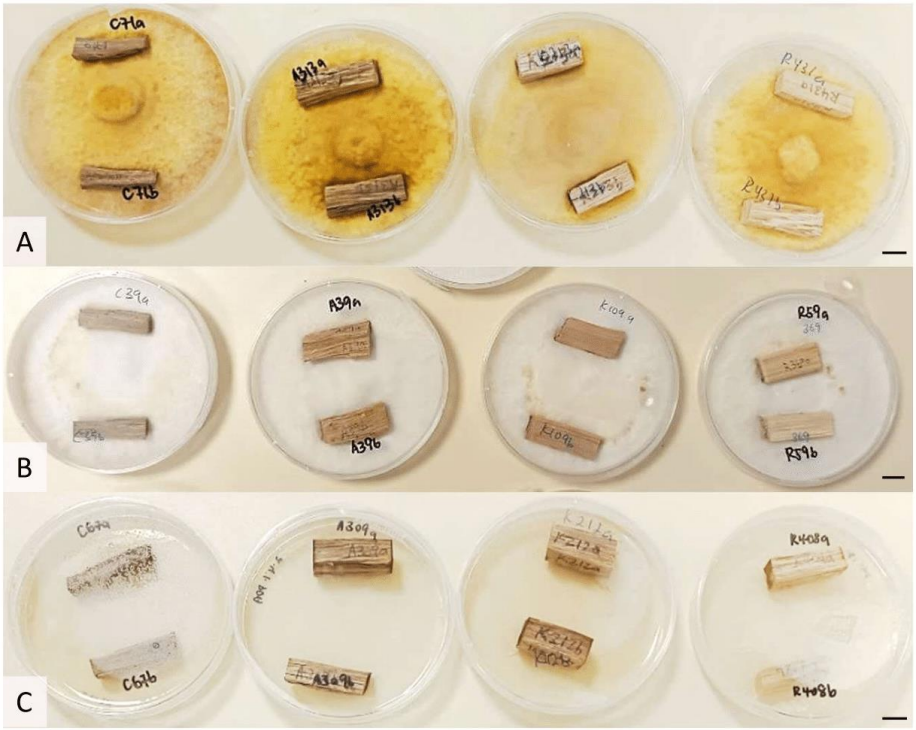

Figure 17: Incubation of wood blocks of four tree species with fungi cultures. From left to right, wood blocks of Casuarina, Angsana, Khaya and Rain tree placed on fungal culture samples *F. siamensis* **(A)**, *R. microporus* **(B)**, and on 2.4% PDA media with antibiotics as the control plates **(C)** on Day 0. Scale bars are 10 mm. Photo credit: Izzah Hazirah bte Junin [80].

3.1.2 Statistical analysis of wood block weight loss after in vitro fungal infection

After the respective incubation period, the fungal mycelia growing on the external surface of the wood blocks were scraped and cleaned using a paper towel (PT Suparma, Tbk, Surabaya, Indonesia) in the biosafety cabinet. The wood blocks were dried in the incubator at 100 °C for 48 h and cooled to room temperature before dry weight change of each wood block were measured with a precision balance. The average percentage dry weight change and standard deviation values for each fungus treatment and tree species combination were calculated using the statistical functions of Microsoft Excel. To assess the significance of the percentage dry weight change after fungal treatment at the different time points of exposure, a one-tailed student's t-test was conducted between the control group and the inoculated group for each species separately.

3.1.3 Volatile-based analysis of in vitro incipient infection in wood blocks

After the respective incubation period, each pair of wood blocks with the removed mycelia from the same culture plate were transferred into a Glad® Quartz-sized Zipper Bag (Glad Products, Oakland, CA, USA), which was then inflated and sealed in the biosafety cabinet to contain 500 mL of head space. For the control samples, the wood blocks were also cleaned using a paper towel to absorb as much moisture as possible and transferred to the Zipper Bags in the same manner. The samples were incubated for 15 min in a dark environment at room temperature before e-nose analysis with six readings per sample of paired wood block and with nitrogen used as the baseline gas.

The e-nose method settings with nitrogen as the baseline purge gas, and downstream evaluation with Canonical Discriminant Analysis (CDA) follows the methodology in subsections 2.1.1 and 2.1.2, except for the steps prior to the generation of the CDA graph. The triplicate sets of six readings were combined into one representative sample class and utilized 10 Principal Components (PCs) (unless stated otherwise).

Selected batches of wood block samples were placed into a 20 mL clear vial capped with 20 mm Viton® Septa Seals (Supelco Inc., Bellefonte, PA, USA) and downstream sampling via SPME-GC-MS were as detailed in subsection 2.1.9.

3.1.4 Basidiocarp and infected tissue (late stage) collection, DNA isolation, barcoding, and volatile-based analysis preparation

A total of 20 fruiting body and wood tissue were collected and processed as detailed in subsection 2.1.5 which included both healthy and diseased samples. Sample barcoding and fungal species identification were conducted as detailed in subsection 2.1.7, and the sample details are listed in Table 5.

Table 5: Samples for e-nose analysis with their molecular identities and sample class names

Sample Number	Type of sample	Host tree	Collection Location	Molecular Identity/GenBank accession no.	Categorised Sample Class
S1	fruiting body	*Syzygium grande*	1°18'38.4"N 103°49'58.6"E	*F. siamensis*/ OQ558845	FS-FB
S2	fruiting body	*Casuarina equisetifolia*	1°17'20.3"N 103°46'12.6"E	*F. siamensis*/ OQ558845	FS-FB
S3	fruiting body	*Casuarina equisetifolia*	1°17'20.3"N 103°46'12.6"E	*F. siamensis*/ OQ558845	FS-FB
S4	fruiting body	*Casuarina equisetifolia*	1°17'20.3"N 103°46'12.6"E	*F. siamensis*/ OQ558845	FS-FB
S5	fruiting body	*Peltophorum pterocarpum*	1°19'14.8"N 103°49'07.8"E	*F. siamensis*/ OQ558845	FS-FB
S6	fruiting body	*Peltophorum pterocarpum*	1°19'14.8"N 103°49'07.8"E	*F. siamensis*/ OQ558845	FS-FB
S7	fruiting body	*Samanea saman*	1°16'58.5"N 103°49'53.9"E	*F. siamensis*/ OQ558845	FS-FB
S8	fruiting body	*Peltophorum pterocarpum*	1°16'56.7"N 103°49'52.4"E	*F. siamensis*/ OQ558845	FS-FB
S9	diseased tissue	*Casuarina equisetifolia*	1°17′20.3″ N 103°46′12.6″ E	*^96.0% F. siamensis/ OQ572588 ^0.4% G. australe/ OQ572592, OQ572594*	FS-DT
S10	diseased tissue	*Tabebuia rosea*	1°19'18.4"N 103°55'31.8"E	*^95.8% F. siamensis/ OQ572588 ^3.60% Fomitiporia bannaensis/ OQ572582*	FS-DT
S11	fruiting body	*Sabal palmetto*	1°19'02.9"N 103°46'09.2"E	*R. microporus/ OQ558868*	RM-FB
S12	fruiting body	*Sabal palmetto*	1°19'02.9"N 103°46'09.2"E	*R. microporus/ OQ558870*	RM-FB
S13	fruiting body	*Wodyetia bifurcata*	1°19'02.6"N 103°46'10.3"E	*^95.6% G. orbiforme/ OQ566787, OQ566786*	GO-FB
S14	fruiting body	*Wodyetia bifurcata*	1°19'02.6"N 103°46'10.3"E	*^96.5% G. orbiforme/ OQ566787, OQ566786*	GO-FB
S15	diseased tissue	*Acoelorrhaphe wrightii*	1°16'54.6"N 103°51'53.4"E	*Ganoderma sp./ OQ558854*	G-DT
S16	fruiting body	*Casuarina equisetifolia*	1°17'20.3"N 103°46'12.6"E	*G. australe/ OQ572592, OQ572594*	GA-FB
S17	fruiting body	*Dypsis lutescens*	1°19'09.0"N 103°46'09.5"E	*G. australe/ OQ558853*	GA-FB
S18	fruiting body	*Peltophorum pterocarpum*	1°18'33.4"N 103°47'59.7"E	*^95.4% P. noxium/ OQ572621, OQ572614*	PN-FB
S19	diseased tissue	*Dypsis lutescens*	1°19'09.0"N 103°46'09.5"E	*^78.5% P. noxium/ OQ572621, OQ572614 ^9.5% G. orbiforme / OQ566787, OQ566786 ^8.4% G. australe /OQ566791, OQ566792*	PNGOGA-DT
S20	healthy tissue	*Casuarina equisetifolia*	1°17'20.3"N 103°46'12.6"E	*N/A*	HT

^ indicates the relative abundance of wood decay fungi in the diseased tissue samples identified through ITS1 metagenomics analysis. Data from Hong et. al [13].

For the e-nose based volatile analysis tests, approximately 40 g (unless stated otherwise) of the sample was placed in a new Glad® Freezer Gallon Zipper Bag (Glad Products, Oakland, CA, USA) and inflated to contain about 2 L of air. The sample was incubated in the bag for 15 min at room temperature, before the samples were analysed with the Cyranose 320 e-nose using the protocol with nitrogen gas as the baseline. The e-nose method settings and downstream evaluation with Canonical Discriminant Analysis (CDA) largely follows the steps described in subsections 2.1.1 and 2.1.2, except for the steps prior to the generation of the CDA graph. Samples molecularly identified as the same pathogen would be combined into one representative 'Categorised Sample Class' (Table 5), and the number of utilized Principal Components (PCs) for dimension reduction was set at ten (unless stated otherwise).

Another 2 g of selected fruiting body and tissue powdered fragments samples were placed into a 20 mL clear vial capped with 20 mm Viton® Septa Seals (Supelco Inc., Bellefonte, PA, USA) and downstream sampling via SPME-GC-MS were as detailed in subsection 2.1.9.

3.1.5 Real-time e-nose species-specific diagnosis of F. siamensis samples

The Cyranose 320 device comes with an on-board diagnostic capability through its "Identify" and "Train" functions. The "Train" function is used initially to create a training model with a limitation of up to six different sample classes, each with a maximum of ten readings taken per sample.

Four *F. siamensis* fruiting body samples (Table 5 samples S5, S6, S7, S8), one *G. australe* fruiting body sample (Table 5 sample S16), and one healthy wood tissue sample (Table 5 sample S20), each with five sample readings, were initially analysed with the e-nose using nitrogen gas as the baseline as detailed in subsection 3.1.4. All five data readings of each sample form a sample class, named as the sample number itself, that was used in the diagnosis training model (Training Model A).

The training model is cross validated before the "Identify" function of the Cyranose 320 can be used to identify an unknown sample against Training Model A. The e-nose snout sampling needle would be inserted into the bag containing the sample-of-interest and stopped at approximately 2 cm away from the sample material during the sample draw step.

When the unknown sample is matched to a sample class in the training model, the e-nose screen shows the corresponding sample class name and an identification quality rating, ranging from the highest confidence of a five-star matching quality (*****), three stars (***), to a one-star low confidence matching quality (*). However, if the unknown sample fails to find a confident match within the sample classes of the training model, the screen will indicate that the sample is "Unknown". During the sample identification process, a canonical algorithm incorporating medium identification quality, auto-scaling, and the Normalization 1 tool was consistently applied.

3.2 Results

3.2.1 Analysis of early stage F. siamensis and R. microporus wood rot sample

The average percentage dry weight change of the wood blocks that were inoculated with *F. siamensis* and *R. microporus*, as well as the control samples, at varying incubation periods of two, four, six, and eight weeks were recorded (Figure 18). At each time point, a pairwise comparison of the weight change of the inoculated samples against the respective control samples was conducted via a one-tailed student's t-test. This would determine if there were significant weight loss due to the wood rot effect of the fungi after a specific incubation period. Generally, it was observed that the samples groups that were exposed to the fungal infection had significant weight loss with p-value less than 0.05 at all four different time points. This was with the exception of the Rain tree and Casuarina samples that had a four week *F. siamensis*-treatment, and Angsana samples that had a two week *R. microporus*

treatment, whereby these groups did not show significant average percentage weight loss when compared with the control groups.

In addition, it was generally observed that longer fungal treatment incubation time results in greater loss in average percentage dry wood weight. For example, Angsana wood block samples treated with *F. siamensis* had an average percentage wood weight reduction of 3.61%, 5.35%, 8.80%, 11.24% after incubation for two, four, six, and eight weeks respectively. The exception to this trend of increased weight loss with increased fungal exposure time was in the Casuarina wood block samples incubated with *F. siamensis* and *R. microporus*, where the average percentage wood weight loss was at the highest at six weeks (6.09% and 8.28% respectively).

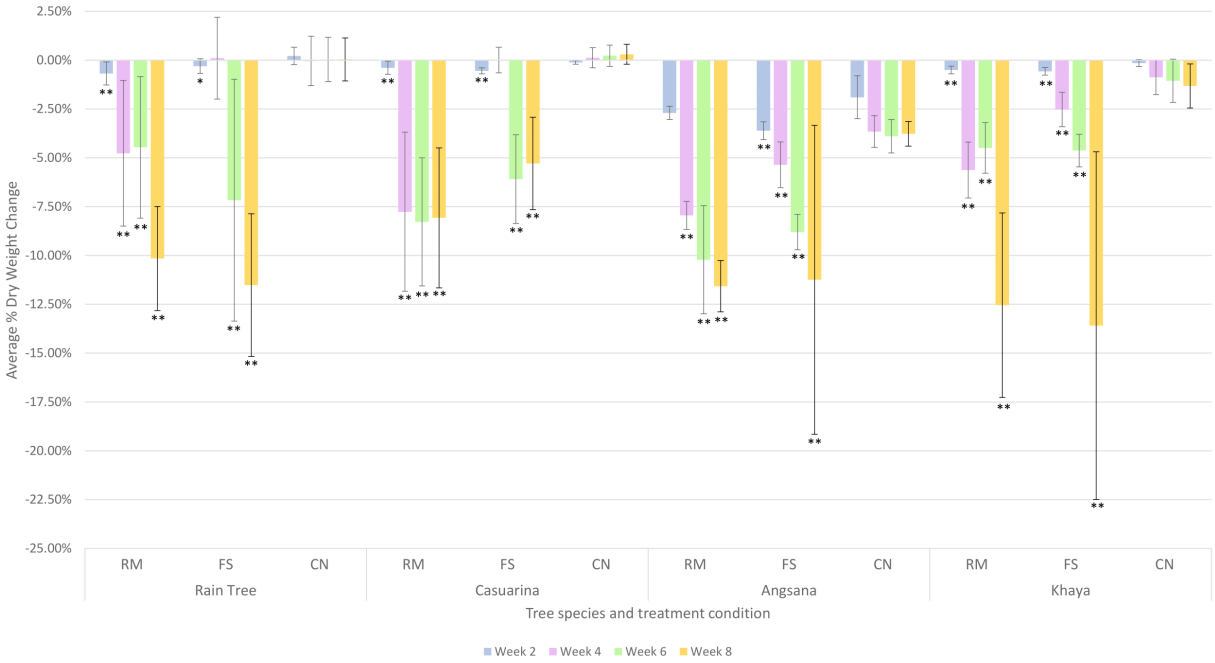

Figure 18: Average percentage dry weight change of wood blocks after fungi treatment for different incubation periods. Wood blocks of four tree species, Rain Tree, Casuarina, Angsana, Khaya (from left to right) were treated with *R. microporus* (RM), or *F. siamensis* (FS), while the control (CN) wood block samples underwent the same procedure but without fungus treatment. Wood blocks were incubated for two, four, six and eight weeks, represented in bar graph colours of blue, pink, green, and yellow respectively. (n = 6). * indicates significant difference between fungal treatment group and corresponding control group by student's t-test ($0.01 < p < 0.05$); ** indicates very significant difference between fungal treatment group and control (CN) group by student's t-test ($p \leq 0.01$). Data assisted by Izzah Hazirah bte Junin [80].

Given that wood decay can start within weeks after fungi exposure, the volatile profiles of these wood block samples were analysed. The e-nose/CDA classification analysis could successfully distinguish between the fungi-treated wood blocks from the control group, as well as differentiate between the different fungi two weeks treatment groups for all four species of wood blocks (Figure 19).

SPME-GC-MS results (Table 6) of the wood block samples supported the e-nose species-specific clustering whereby samples treated with *F. siamensis* had uniquely high amounts of 1,2,4,5-tetrachloro-3,6-dimethoxybenzene (abundance more than 20%) and 1,4-dichloro-2,5-dimethoxybenzene (abundance 5-10%). The samples treated with *R. microporus* had varying unique and high abundance volatiles (at least 5% in abundance) specific to the tree species, for example the Angsana wood block treated with *R. microporus* emitted high amounts of benzaldehyde (abundance more than 20%), whereas the Khaya wood block emitted high amounts of (4aR,5S)-5,8-Diethyl-6-methylene-1,2,3,4,4a,5,6,7-octahydro-naphthalene (abundance 10-20%), Rain tree wood block with beta-funebrene (abundance 5-10%). 1-methyl-4-(1,2,2-trimethylcyclopentyl)-benzene appears to be a unique volatile specific to three out of four tree species of the *R. microporus*-treated blocks but varied in abundance across the three species: Khaya with the least at less than 0.1-1%, Rain tree at 1-5%, and Casuarina at 5-10% in abundance.

The e-nose/CDA classification analysis could also discriminate the samples based on incubation time for tree species of Angsana (Figure 20), Casuarina and Rain tree (Appendix B) under both fungal treatments, with MDist above 5.000. Khaya samples treated with *F. siamensis* could not be clearly distinguished based on incubation time, with pairwise comparison of the samples from the two weeks (K-FS-2w) and eight weeks (K-FS-8w) incubation period having an MDist of 4.330 (Appendix B).

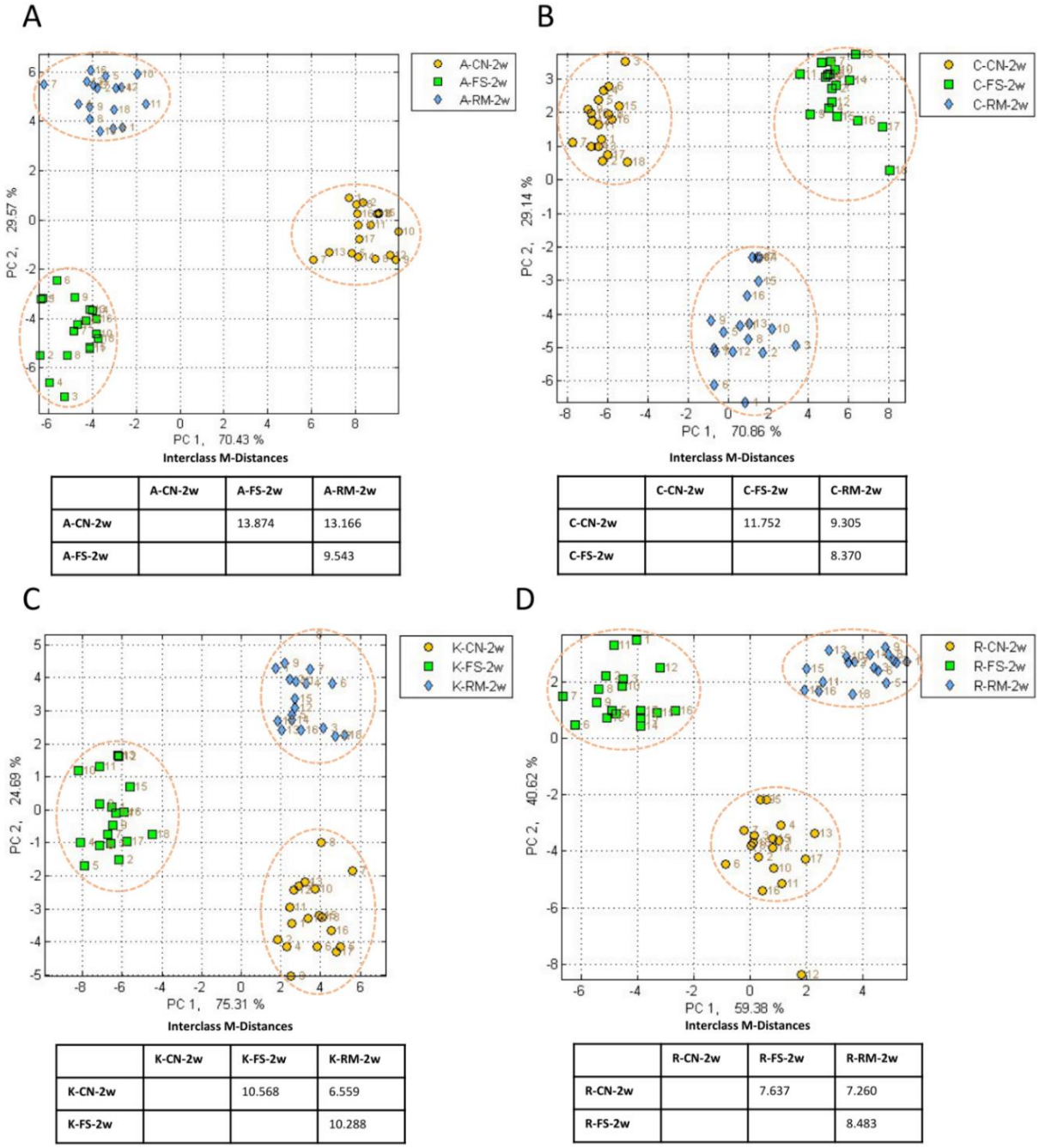

	A-CN-2w	A-FS-2w	A-RM-2w
A-CN-2w		13.874	13.166
A-FS-2w			9.543

	C-CN-2w	C-FS-2w	C-RM-2w
C-CN-2w		11.752	9.305
C-FS-2w			8.370

	K-CN-2w	K-FS-2w	K-RM-2w
K-CN-2w		10.568	6.559
K-FS-2w			10.288

	R-CN-2w	R-FS-2w	R-RM-2w
R-CN-2w		7.637	7.260
R-FS-2w			8.483

Figure 19: Scatter plots with Canonical Discriminant Analysis (CDA) and calculated Interclass M-Distances (MDist) on e-nose volatile readings of four tree species after two weeks incubation of wood rot fungi. A: Volatile classification by the e-nose of wood blocks of Angsana tree with two weeks of fungal treatment of *F. siamensis* (A-FS-2w), *R. microporus* (A-RM-2w), and control samples with no fungal treatment (A-CN-2w); **B**: Volatile classification by the e-nose of wood blocks of Casuarina tree with two weeks of fungal treatment of *F. siamensis* (C-FS-2w), *R. microporus* (C-RM-2w), and control samples with no fungal treatment (C-CN-2w); **C**: Volatile classification by the e-nose of wood blocks of Khaya tree with two weeks of fungal treatment of *F. siamensis* (K-FS-2w), *R. microporus* (K-RM-2w), and control samples with no fungal treatment (K-CN-2w); **D**: Volatile classification by the e-nose of wood blocks of Rain tree with two weeks of fungal treatment of *F. siamensis* (R-FS-2w), *R. microporus* (R-RM-2w), and control samples with no fungal treatment (R-CN-2w). Samples inside an orange dashed-line ellipse indicate that the MDist is greater than 5.000 and thus form a distinctive cluster.

Table 6: Volatiles of selected wood block samples with fungal treatment identified by SPME-GC-MS

Volatile	CAS No.	R-RM*	K-RM*	C-RM*	A-RM*	R-FS*	K-FS*	C-FS*	A-FS*
(1R,4R,5S)-1,8-Dimethyl-4-(prop-1-en-2-yl)spiro[4.5]dec-7-ene	729602-94-2	*		**					
(3aR,4R,8R,8aS)-3a,4,7,8a-Tetramethyl-1,2,3,3a,4,5,8,8a-octahydro-4,8-methanoazulene	053060-59-6			**				*	
(3aR,4R,8R,8aS)-3a,4,8a-Trimethyl-7-methylenedecahydro-4,8-methanoazulene-rel	072346-55-5		**	***			*	*	
(4aR,5S)-5,8-Diethyl-6-methylene-1,2,3,4,4a,5,6,7-octahydro-naphthalene	997220-37-8		****						
(4aS,8aS)-1,1,4a-trimethyl-5,6-dimethylene-decalin	058795-27-0		**						
(E)-Oct-2-enal	002363-89-5				**				
(R)-1-Methyl-4-(6-methylhept-5-en-2-yl)cyclohexa-1,4-diene	028976-67-2		**						
1H-3a,7-Methanoazulene, octahydro-3,8,8-trimethyl-6-methylene-, [3R-(3.alpha.,3a.beta.,7.beta.,8a.alpha.)]-	000546-28-1		**	**					
2-(1,3-Benzodioxol-5-ylmethyl)-1H-isoindole-1,3(2H)-dione	997493-03-6			**			**		
2,4-bis(chloranyl)-1,5-dimethoxy-3-methyl-benzene	997271-90-6					**	*		
2,4-Dichloro-5-fluoroacetophenone	000704-10-9					**			
2-Benzylidenehydrazono-3-methyl-2,3-dihydrobenzothiazole	997443-22-4					*	*	*	*
3,5-bis(chloranyl)-2,4-dimethoxy-6-methyl-phenol	997329-33-1					*	*	*	*
3-Isopropyl-6,8a-dimethyl-1,2,4,5,8,8a-hexahydroazulene	016661-00-0			**					
alpha-cuprenene	029621-78-1	**		**					
alpha-muurolene	010208-80-7		*			*	*	*	
Benzaldehyde	000100-52-7		**		*****				
Benzene, 1-(1,5-dimethyl-4-hexenyl)-4-methyl	000644-30-4	*	***	**	*	*	*	*	*
Benzene, 1-(1,5-dimethylhexyl)-4-methyl	001461-02-5		**						
Benzene, 1,2,4,5-tetrachloro-3,6-dimethoxy-	000944-78-5					*****	*****	*****	*****
Benzene, 1,4-dichloro-2,5-dimethoxy-	002675-77-6					***	***	***	***
Benzene, 1-methyl-4-(1,2,2-trimethylcyclopentyl)-, (R)	016982-00-6	**	*	***					
Benzene, ethenyl-	000100-42-5	**							
beta-farnesene	018794-84-8			*		**	*	*	
beta-funebrene	079120-98-2	***							
Bicyclogermacrene	100762-46-7			**					
Dodecane	000112-40-3	*	**	*	**	*	*	*	
Furan, 2-pentyl-	003777-69-3				**				
Hexanoic acid, 2-ethyl-, methyl ester	000816-19-3				**				
Nonanal	000124-19-6				**				
Oxime-, methoxy-phenyl-	997073-83-3	**	*		**				
Tricyclo[2.2.1.0(2,6)]heptane, 1,7-dimethyl-7-(4-methyl-3-pentenyl)-, (-)	000512-61-8		**						

Legend: Relative abundance — < 0.1%; * 0.1–1%; ** 1–5%; *** 5–10%; **** 10–20%; ***** > 20%

*****Abbreviations: FS for *F. siamensis*; RM for *R. microporus*; R for Rain tree wood blocks; K for Khaya wood blocks; C for Casuarina wood blocks; A for Angsana wood blocks

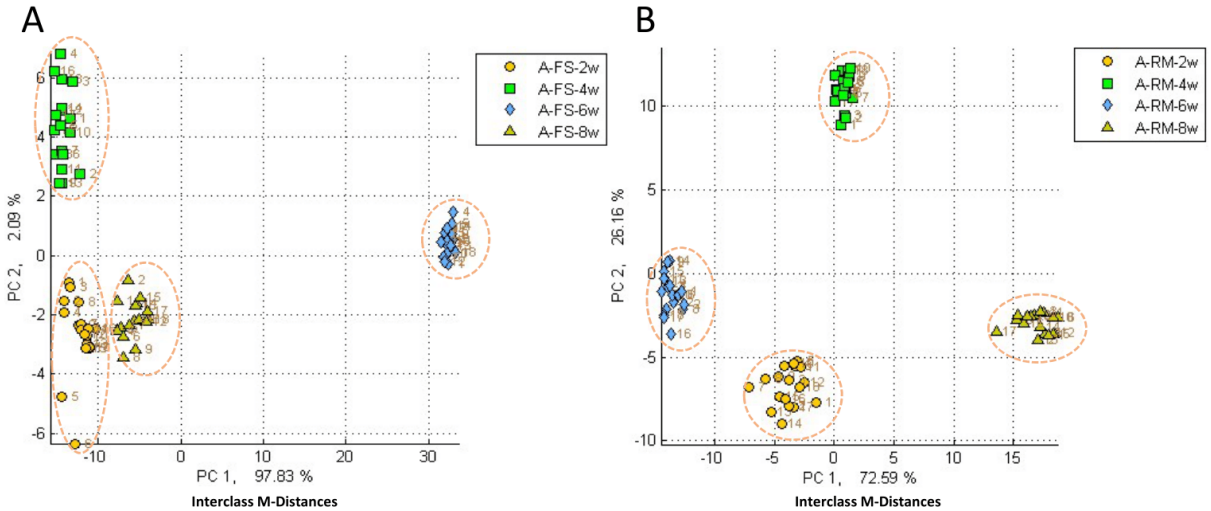

Interclass M-Distances

	A-FS-2w	A-FS-4w	A-FS-6w	A-FS-8w
A-FS-2w		7.308	44.771	6.556
A-FS-4w			46.844	10.652
A-FS-6w				38.387

Interclass M-Distances

	A-RM-2w	A-RM-4w	A-RM-6w	A-RM-8w
A-RM-2w		18.419	11.878	21.433
A-RM-4w			19.116	21.527
A-RM-6w				30.776

Figure 20: Scatter plots with Canonical Discriminant Analysis (CDA) and calculated Interclass M-Distances (MDist) on e-nose volatile readings of Angsana wood blocks exposed to wood rot fungi. A: Volatile classification by the e-nose of wood blocks of Angsana tree with two weeks (A-FS-2w), four weeks (A-FS-4w), six weeks (A-FS-6w), eight weeks (A-FS-8w) of fungal treatment with *F. siamensis*; **B**: Volatile classification by the e-nose of wood blocks of Angsana tree with two weeks (A-RM-2w), four weeks (A-RM-4w), six weeks (A-RM-6w), eight weeks (A-RM-8w) of fungal treatment with *R. microporus*. Samples inside an orange dashed-line ellipse indicate that the MDist is greater than 5.000 and thus form a distinctive cluster.

3.2.2 Late stage wood rot infection species-specific volatile classification

Based on the sensor reading pattern data, all eight *F. siamensis* fruiting bodies were collated into one sample class (FS-FB). Similarly, the data of all *R. microporus*, *G. australe*, *G. orbiforme*, and *P. noxium* fruiting bodies (Table 5) were collated into one sample class per species (RM-FB, GA-FB, GO-FB, PN-FB respectively). CDA classification with ten PCs could distinguish all species of fruiting body samples with MDist larger than 5.000 (Figure 21A), except for the *R. microporus* and *G. orbiforme* sample classes with an MDist of 1.090.

Two *F. siamensis* infected diseased tissues (FS-DT), one Ganoderma infected diseased tissue (G-DT) was selected for e-nose analysis. One diseased tissue infected with *G. australe, G. orbiforme* and *P. noxium* (PNGOGA-DT), and one healthy Casuarina tree wood tissue (HT) were also included as an outlier and sample reference class respectively. The specific fungal composition of the samples is detailed in Table 5. At ten PCs for dimension reduction in CDA, the results could show clear distinction between the healthy tissue sample and the infected samples with large MDist of greater than 5.000 (Figure 21B).

SPME-GC-MS analysis revealed the identity of volatiles in the fruiting body and diseased tissue samples (Table 7). Notably, a major volatile compound, 1,2,4,5-tetrachloro-3,6-dimethoxybenzene, was consistently detected in all tested *F. siamensis* basidiocarp (Table 7, S1, S2, S4, S6, S7) and diseased tissue samples (Table 7, S10) in high abundance but was absent in the *G. australe* and *R. microporus* samples. Diethyl phthalate was present in high abundance (10-20%) in *G. australe* fruiting body (Table 7, S16), while dimethyl disulfide was present in high abundance (10-20%) in *R. microporus* fruiting body (Table 7, S11).

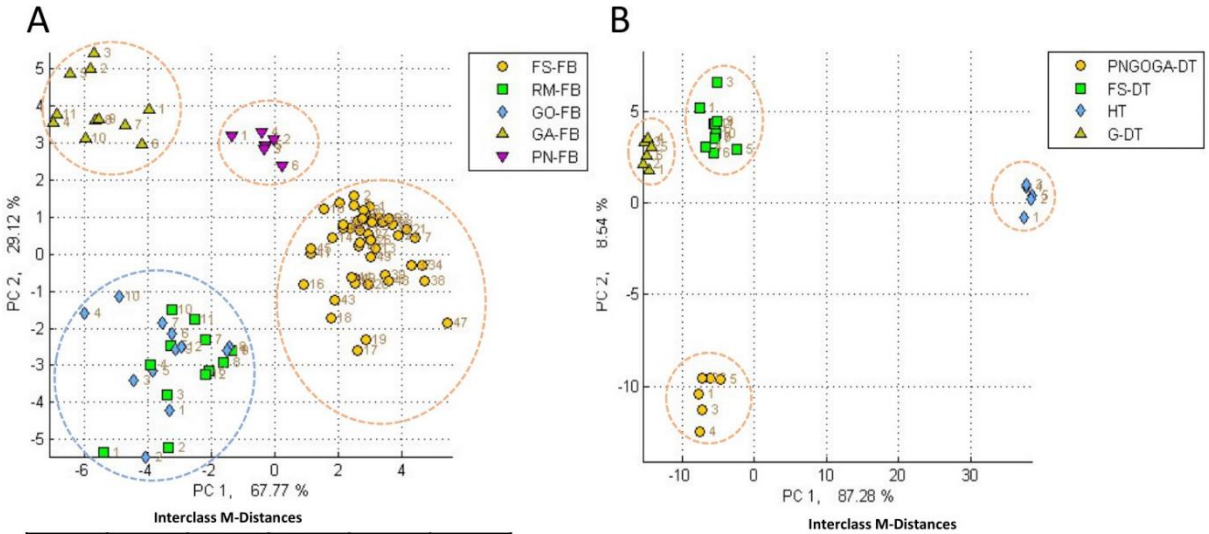

Interclass M-Distances

	FS-FB	RM-FB	GO-FB	GA-FB	PN-FB
FS-FB		6.676	7.089	9.332	5.008
RM-FB			1.090	7.635	6.948
GO-FB				7.095	6.950
GA-FB					6.187

Interclass M-Distances

	PNGOGA-DT	FS-DT	HT	G-DT
PNGOGA-DT		14.886	45.933	17.222
FS-DT			43.765	14.019
HT				52.923

Figure 21: Scatter plots with Canonical Discriminant Analysis (CDA) and calculated Interclass M-Distances (MDist) on e-nose volatile readings of varying late stage disease samples infected by varying fungal pathogens. A: Volatile classification by the e-nose of basidiocarps *F. siamensis* (FS-FB), *R. microporus* (RM-FB), *G. orbiforme* (GO-FB), *G. australe* (GA-FB), and *P. noxium* (PN-FB); **B**: Volatile classification by the e-nose of infected wood tissues with *P. noxium*, *G. orbiforme*, *G. australe* (PNGOGA-DT), *F. siamensis* (FS-DT), *Ganoderma sp.* (G-DT) and a control healthy tissue sample (HT). Samples inside an orange dashed-line ellipse indicate that the MDist is greater than 5.000 and thus form a distinctive cluster. Samples inside a blue dashed-line ellipse indicates a cluster of two samples with MDist less than 5.000, which is also indicated in blue in the pairwise comparison Interclass M-Distances table.

Table 7: Volatiles of selected fruiting body and wood tissue samples identified by SPME-GC-MS

Volatile	CAS No.	*S10 (FS-DT)**	*S1 (FS-FB)**	*S2 (FS-FB)**	*S4 (FS-FB)**	*S6 (FS-FB)**	*S7 (FS-FB)**	*S16 (GA-FB)**	*S11 (RM-FB)**
(3aS,8aS)-6,8a-Dimethyl-3-(propan-2-ylidene)-1,2,3,3a,4,5,8,8a-octahydroazulene	395070-76-5	**				*	*		
3,5-bis(chloranyl)-2,4-dimethoxy-6-methyl-phenol	997329-33-1	**		**		**	*		
3-Octanone	000106-68-3				*		**		
Acetic acid	000064-19-7		***					**	
Benzene, 1-(1,5-dimethyl-4-hexenyl)-4-methyl	000644-30-4					*			
Benzene, 1,2,4,5-tetrachloro-3,6-dimethoxy-	000944-78-5	*****	*****	*****	*****	*****	*****		
Benzene, 1,2,4-trichloro-5-nitro-	000089-69-0					*****			
Benzene, 1,3-dimethyl-	000108-38-3	*					*		**
Benzene, 1,4-dichloro-2,5-dimethoxy-	002675-77-6	**		*		**	***		
beta-Bisabolene	000495-61-4	**	*						
beta-Farnesene	018794-84-8	***				*	*		
Butyrolactone	000096-48-0						**		
Diethyl Phthalate	000084-66-2		*					****	
Disulfide, dimethyl	000624-92-0								****
Docosane	000629-97-0							**	
Nonanal	000124-19-6		*				*		
Phenol, 2,3,5,6-tetrachloro-4-methoxy	000484-67-3		*				**		
Phenylethyl Alcohol	000060-12-8								**
Toluene	000108-88-3	*	*	*			*	*	**

Legend

Relative abundance	
	< 0.1%
*	0.1–1%
**	1–5%
***	5–10%
****	10–20%
*****	> 20%

*****Abbreviations: FS-DT for *F. siamensis infected diseased tissue*, FS-FB for *F. siamensis* fruiting body, GA-FB for *G. australe* fruiting body, RM-FB for *R. microporus* fruiting body. Adapted from Tan et. al [81].

3.2.3 Real time volatile-based species-specific identification of F. siamensis

A *F. siamensis*-specific training model – Training Model A, was created for species-specific identification in the field. Training Model A included four *F. siamensis* fruiting body samples (Table 5 samples S5, S6, S7, S8), which were selected as the reference classes to ensure the training model had sufficient representation of *F. siamensis* fruiting body samples from the host tree species that were inspected (i.e. *Peltophorum pterocarpum, Samanea saman*). One *G. australe* fruiting body sample (Table 5 sample S16), and one healthy wood tissue sample (Table 5 sample S20) were included in the training model as a reference point for another wood rot fungi species, and as the control to represent a healthy-state sample respectively.

The e-nose, equipped with Training Model A, was assessed for its applicability in diagnosing *F. siamensis* fruiting bodies in field settings. Suspected *F. siamensis* fruiting bodies were discovered in one *Samanea saman* tree (R1) and two *Peltophorum pterocarpum* trees (Y1 and Y2). To examine the potential influence of sample size on e-nose diagnosis, one large piece (R1-A, YF1-A, YF2-A) and one small piece (R1-B, YF1-B, YF2-B) of the suspected fruiting bodies were collected from each tree. The samples were placed in a Glad® Freezer Gallon Zipper Bag and the sample volatiles were allowed the equilibrate in the bag for 15 min before e-nose testing with nitrogen as the baseline gas using the "Identify" tool as described in subsection 3.1.5 and the set-up is depicted in Figure 22.

Additionally, the air near the *Peltophorum pterocarpum* tree (YF2) was tested by directing the e-nose needle near the tree stump without any surrounding fruiting bodies, serving as a negative reference point. Utilising the on-board e-nose "Identify" tool, all tested samples were identified as a *F. siamensis* fruiting body training sample class, specifically sample S5 (Table 5), with varying levels of confidence (Table 8).

Figure 22: E-nose set-up of the real time field prediction of unknown sample with nitrogen gas used as the baseline gas. Adapted from Tan et. al [81].

Table 8: Identification results of fruiting body samples via Cyranose 320 on-board Identification tool

Sample Name	Host Tree	Fruiting Body Weight (g)	E-Nose Diagnosis Result (Confidence)	Molecular Identity by Barcoding
R1-A	*Samanea saman*	104.50	S5 (*****)	*F. siamensis*
R1-B	*Samanea saman*	5.33	S5 (*****)	*F. siamensis*
YF1-A	*Peltophorum pterocarpum*	336.14	S5 (*****)	*F. siamensis*
YF1-B	*Peltophorum pterocarpum*	12.14	S5 (*)	*F. siamensis*
YF2-A	*Peltophorum pterocarpum*	191.17	S5 (*****)	*F. siamensis*
YF2-B	*Peltophorum pterocarpum*	15.44	S5 (***)	*F. siamensis*
YF2 Tree Stump	*Peltophorum pterocarpum*	Negative Control	Unknown	-

Adapted from Tan et. al [81].

3.3 Discussion

This chapter demonstrated that *F. siamensis* and *R. microporus* have a significant degree of pathogenicity in causing wood weight loss of four commonly planted urban tree species from as early as two weeks of incubation. An exception was *R. microporus* on Angsana which started significant dry weight loss only at the four week incubation (Figure 18). As the treatment incubation period increases, the average percentage of dry weight loss of the wood blocks generally increases. The insignificant change in weight after four week incubation of

Rain tree and Casuarina samples by *F. siamensis* could be due to slow initial progression in pathogenesis. Overall, this shows that the presence of *F. siamensis* or *R. microporus* mycelia within the wood tissues of these four species could do damage within a short span of time, and that the reliance on visual assessments of the formation of fruiting bodies for wood decay diagnosis may be ineffective for early stage disease diagnosis.

Volatile analysis of the wood blocks after the externally growing fungal mycelia have been stripped off would ensure that the volatiles released by the samples are from the wood after infection and the fungi mycelia that have penetrated to the core of the wood block, closer to what happens in a natural infection. This experiment investigates the sensitivity of the volatile-based tools to differentiate between two species of fungal-treated wood blocks at an early infection stage, as early as two weeks after treatment. The e-nose/CDA classification analysis results shows that there is sufficient sensitivity in discriminating the wood blocks that were fungi-treated for two weeks from the control healthy reference group (Figure 19). SPME-GC-MS results reveal that *F. siamensis*-treated samples have two unique volatiles in large abundance – 1,2,4,5-tetrachloro-3,6-dimethoxybenzene ($C_8H_6Cl_4O_2$) and 1,4-dichloro-2,5-dimethoxybenzene ($C_8H_8Cl_2O_2$), with more than 20% abundance and 5-10% abundance respectively (Table 6), which may underline clear discrimination of the *F. siamensis*-treated group from the *R. microporus*-treated group and the control reference group. These two volatiles were also found to be present in the *F. siamensis* mycelia cut plug samples results (Table 4), with the volatile 1,2,4,5-tetrachloro-3,6-dimethoxybenzene having >20% of the total volatile abundance, while 1,4-dichloro-2,5-dimethoxybenzene was in a small abundance of 0.1-1%. Notably, 1,4-dichloro-2,5-dimethoxybenzene, also known as Chloroneb, was present in much higher amounts in the wood block-treatment samples, possibly due to the fungi interactions with the wood blocks. Chloroneb, is a selective fungicide against oomycetes such as *Phytophthora*, *Pythium*; *Mucor* (a Phycomycete); and *Botrytis* (a

Leotiomycetes). It acts on the lysis of membrane organelles such as mitochondria and nucleus of sensitive fungi strains and can inhibit DNA, RNA and protein synthesis [98]. However, resistant fungi strains have been reported [98,99]. This compound may give *F. siamensis* a competitive advantage over other fungi while serving as a signature volatile for early stage diagnosis. On the other hand, it may be useful for screening its species specific biocontrol agents.

For *R. microporus*, GC-MS volatile analysis of wood block samples of Khaya, Rain tree and Casuarina after treatment identified the common presence of 1-methyl-4-(1,2,2-trimethylcyclopentyl)-benzene ($C_{15}H_{22}$), also known as cuparene, a sesquiterpene. Cuparene derivatives are reported to serve antimicrobial functions against fungi such as *Cladosporium herbarum*, and bacteria such as *Bacillus subtilis* and *Staphylococcus aureus*. It was isolated from the *Flammulina velutipes* (an Agaricomycetes) culture [100], and from plant such as *Hypericum scabrum* and *Juniperus occidentalis* [101] could contribute to their natural defence mechanism [102]. This volatile was present in varying abundance amongst the samples which may indicate that the host-fungi interactions affect its volatile concentrations.

Unique host-fungi combination specific volatiles were also detected. Beta-funebrene ($C_{15}H_{24}$) was a volatile unique to Rain tree wood blocks inoculated with *R. microporus.* Similar to Cuparene, funebrene derivatives are sesquiterpenes that may be involved in the defence mechanism and have been found in volatile analysis of both fungi [103] and plants [104]. Similarly, *R. microporus*-treated Khaya wood block emitted high amounts (abundance 10-20%) of (4aR,5S)-5,8-Diethyl-6-methylene-1,2,3,4,4a,5,6,7-octahydro-naphthalene ($C_{15}H_{24}$) which is also a sesquiterpene derivative. Angsana wood block treated with *R. microporus* emitted high amounts of benzaldehyde (C_7H_6O) (abundance > 20%), a molecule which have been found to be produced by wood decay fungi such as Polyporales *Fomes fomentarius* [105]. Such host tree specific variation in volatile profiles after *R. microporus* infection could

pose a challenge or interference to *R. microporus* e-nose based diagnosis or other devices based on response patterns of sensors. For the situation of less fungus species specific volatiles and more host tree dependent volatiles, SPME-GC-MS will be more suitable since the fungus specific volatile can be clearly identified and mainly used to conclude a diagnosis.

Apart from fungus species-specific differentiation, the same fungi-treated wood blocks of different disease progression stage can also be distinguished by the e-nose (Figure 20). In addition, SPME-GC-MS results demonstrated that the volatile profiles of field samples of late stage infection (Table 7) were different from those of early stage infection (Table 4, Table 6), especially for *R. microporus* samples. *R. microporus* fruiting body volatile profile by SPME-GC-MS revealed high abundance of antifungal compound, dimethyl disulfide ($C_2H_6S_2$) which is reportedly also produced by few fungi species such as *Fusarium*, *Penicillium* and *Trichoderma* [72]. This volatile was not previously detected in the fungi-treated wood block samples of the *in vitro* pathogenesis study (Table 6) or in the pure fungal mycelia sample (Table 4). This implies that there are changes in the volatile composition during different stages of *R. microporus* fungi growth and disease development. Hence, early diagnosis of *R. microporus* by e-nose needs a separate model, followed by validation of a reasonable number of samples.

In subsection 3.2.3, the volatile profile data during the training stage was used to create a training model (Training Model A) and utilised for real time field application of volatile-based diagnosis on *F. siamensis* fruiting bodies. The created model was loaded onto the e-nose tool and this model could successfully be used to identify the fruiting body samples of varying amounts from the three different trees (R1, YF1, YF2). These samples were also validated by molecular methods to be *F. siamensis.* Notably, the prediction results of the samples with lower amounts of fruiting bodies (YF1-B and YF2-B) had a confidence rating lower than that of the larger amounts (YF1-A and YF2-A). The smaller quantity of fruiting

bodies enclosed in the bag could have influenced the concentration of volatiles in the headspace, potentially leading to a decrease in the confidence level during the diagnosis test. This sample quantity dependent variation in diagnosis confidence suggests the need for a minimum sample quantity for field diagnosis and the exact minimum quantity for each fungus might vary. On the other hand, smaller amount of sample might need a longer incubation period for reliable diagnosis.

The success of volatile-based diagnosis of *F. siamensis* could be attributed to the emission of high abundance volatiles that are unique to this fungus and consistently present in all infected plants. This work demonstrates that volatile 1,2,4,5-tetrachloro-3,6-dimethoxybenzene can be species-specific identifier or marker for *F. siamensis*. For those fungi without such single molecule identifier, diagnosis is still possible with the recognition of profiles of volatiles by GC-MS analysis.

Chapter 4: General Discussion

Traditional identification of wood rot fungi is often attributed to the visual inspections of late stage fruiting body growth identification or require laboratory barcoding via DNA extraction and downstream sequencing which are time-consuming. This thesis demonstrates a new approach using volatile-based techniques to differentiate the six wood rot fungi species, as pure cultures as well in diseased tissues as early as two weeks after infection. It opens the door to utilise volatile-based tools for early stage diagnosis of wood decay in Singapore.

To identify unique volatiles associated with the six fungi species and their infection, cultures and diseased wood samples were analysed by SPME-GC-MS, which can identify chemical structures through comparison of MS spectra against the NIST Mass Spectral Database. The results reveal the distinct volatile profiles of different fungi species as well as various host tree-fungi combination. Such distinct volatile profiles could also be differentiated by the e-nose. Notably, the volatile profiles of all types of *F. siamensis* samples consistently exhibit a high abundance (greater than 20%) of 1,2,4,5-tetrachloro-3,6-dimethoxybenzene, a key signature volatile absent in other tested fungal wood rot pathogens. This consistent and dominant common volatile for *F. siamensis* underlines the volatile-based diagnosis for this fungus, which overcomes the difficulty in morphology-based diagnosis brought by its morphological plasticity of the basidiocarps.

Prior research predominantly employed ambient air for the purging step when using e-noses to detect plant diseases, as referenced in studies [59,66,106]. This thesis presents a significant advancement in the field of electronic nose (e-nose) technology – using nitrogen gas to purge the e-nose sensors substantially enhances its sensitivity in classifying volatiles related to wood rot (detailed in subsection 2.2.2). Moreover, the practicality of this approach is further enhanced by integrating a portable nitrogen gas pouch, making it highly feasible for on-site

tree assessments. This study showed that with the optimised nitrogen gas protocol and CDA classification algorithm, it was possible to achieve species-specific classification of volatile profiles of the six prevalent wood rot fungal species – *F. siamensis*, *R. microporus*, *P. noxium*, *G. australe*, *G. orbiforme*, and *L. theobromae* cultivated on agar. Furthermore, the effectiveness of volatile-based tools is not confined to laboratory conditions but extends to field applications.

The study indicates that soil-type samples are less ideal for e-nose due to the dilution of signature volatiles, whereas wood tissues and fungi fruiting bodies are highly suitable for volatile-based wood rot disease tests. Remarkably, wood rot infection of *in vitro* infected wood tissue samples can be detected as early as two weeks post-treatment (subsection 3.2.1). This finding is particularly significant as it demonstrates that volatile-based analysis can potentially detect very early stage wood rot, prior to any visual signs of wood decay.

Building on the significant advancements demonstrated in this thesis, it's crucial to acknowledge the current limitations of the e-nose technology, especially when considering its application for the efficient and cost-effective diagnosis of wood-rot fungi. Despite its promising capabilities, there are specific challenges that need to be addressed. One of the primary limitations is the Cyranose 320 e-nose's restricted capacity for reference classes, which currently stands at a maximum of six. This constraint necessitates a strategic selection of reference samples to construct the most effective and suitable model for each specific host-fungal species combination. This selection process is critical to ensure the accuracy and effectiveness of the e-nose in various scenarios. Additionally, the e-nose's ability to cluster data based on the stage of infection underscores the need for a diverse and comprehensive training dataset that includes samples from various stages of infection. Such a dataset would enhance the e-nose's precision in identifying and categorizing different stages of wood rot. Despite the model building restrictions, this thesis displayed the possibility of successful

model creations with the choice of late stage basidiocarp samples to build the training model for the field investigation of *F. siamensis* basidiocarp identification in *Samanea saman* and *Peltophorum pterocarpum* host trees.

Another challenge arises from the fact that not all pathogen-host combinations are amenable to species-specific diagnosis through volatile-based methods by e-nose. This is partly due to the absence of a universally abundant volatile compound across all fungi species. Furthermore, situations of co-infection or secondary infections by multiple wood rot fungi species within a single host can further complicate the process of achieving a species-specific diagnosis. An example of this complexity is evident in sample S19 (referenced in Table 5), where three different fungal species were identified within the diseased wood tissue, illustrating the intricate nature of these infections. To overcome this challenge, training the e-nose with more samples that are co-infected by different wood rot fungi could help to build a better, encompassing model to consider these unique scenarios. For variation of volatile profiles heavily influenced by host tree or complicated by the presence of multiple pathogens, GC-MS could be a better choice. On the other hand, volatile based diagnosis may need confirmation of other complementary techniques like DNA based diagnosis.

Despite these challenges to volatile based diagnosis, this thesis has developed a protocol that enhanced the use of the e-nose, which demonstrated remarkable sensitivity in confidently identifying and differentiating infected samples, even at the early, incipient stages of infection. Volatile-based techniques can provide invaluable assistance for field investigations as it offers a significant advantage over traditional methods, which often rely on visual assessments or more invasive techniques such as resistance drilling. The ability to detect infections at an early stage, with minimal disruption to the host, highlights volatile-based diagnosis as a potential cutting-edge tool in the field of plant pathology and wood rot detection.

Chapter 5: Conclusion

Wood rot infection by fungi species of *F. siamensis, R. microporus, P. noxium, G. orbiforme, G. australe,* and *L. theobromae* were demonstrated to release unique volatiles that can be detected. This thesis found that the use of nitrogen gas to purge the residual volatiles from the e-nose sensors and to set the baseline improved the sensor response to the sample analytes. This should be set as a new standard protocol by using nitrogen gas rather than ambient gas. With this set up, subsequent volatile profile classification analysis displayed good sensitivity and specificity in distinguishing plant/fungi-related volatiles, the six different species of wood rot fungi, as well as *F. siamensis* and *R. microporus*-treated wood blocks from as early as two weeks post-treatment. This demonstrated that volatile-based methods can assist in species-specific and early stage diagnosis of wood rot disease in trees. Moreover, field application of volatile detection tools was shown to be convenient and successful – the e-nose could be used on-site to identify *F. siamensis* fruiting bodies in the field settings with minimal sample preparation costs (20 mL of nitrogen gas per reading and sample bags), quick incubation time (15 min) and rapid response time (less than one min).

In summary, this study explored the application of two complementary volatile-based detection techniques (e-nose and SPME-GC-MS) on wood rot diagnosis and introduced a new approach of using nitrogen gas with the e-nose baseline purge step. Application of volatile-based diagnosis is expected to facilitate early detection, prompt timely intervention, and help effective control of fungal diseases, hence help urban forestry management in the future.

Contributions and Acknowledgement of Funding

Investigation and data from Figure 9, 17, 18, 19, 20, Appendix B was assisted by Final Year Project student Izzah Hazirah bte Junin [80]; data from Figure 1 and Table 5, pictures from Figure 2, 3, 4, 5 was obtained from Hong et. al [13]; and data of Figure 10, 11, 12, 16, 22, Table 7, Table 8, Appendix A were, prior to the final submission of this thesis, published as a first author in Tan et. al [81].

This research was funded by The Ministry of National Development Research Fund/National Parks Board Singapore to Hong Y., Mutwil M., and Chan P.M. (Grant number NTU REF 2019-1120). It was also partially supported by School of Biological Sciences, Nanyang Technological University Final Year Project (FYP) funds for Izzah H.J.

References

1. O'Neill, J. The garden city in Singapore. In *The Culture of Nature in the History of Design*, Fallan, K., Ed.; Routledge: London, 2019; pp. 89-102.
2. Tee, S.P.; Wee, M.L.; Low, Y.K. *Trees of our garden city: A guide to the common trees of Singapore*; Draco Pub: 2001.
3. Aldous, D.E. Planning Green Open Spaces for South East Asian Capital Cities. *Parks - Enhancing Liveability in Cities* **2011**, *3*, 10-15.
4. Tan, A. Not a concrete jungle: Singapore beats 16 cities in green urban areas. *The Straits Times* 2017.
5. Tan, C. 80,000 more trees to be planted by 2030 to cool industrial estates: Tan Kiat How. *The Straits Times* 2022.
6. Downer, A.J.; Perry, E.J. Wood Decay Fungi in Landscape Trees. Available online: http://ipm.ucanr.edu/PMG/PESTNOTES/pn74109.html (accessed on
7. Shortle, W.C.; Dudzik, K.R. *Wood decay in living and dead trees: A pictorial overview*; U.S. Department of Agriculture, Forest Service, Northern Research Station: 2012.
8. Ann, P.-J.; Chang, T.-T.; Ko, W.-H. Phellinus noxius Brown Root Rot of Fruit and Ornamental Trees in Taiwan. *Plant Disease* **2002**, *86*, 820-826, doi:10.1094/pdis.2002.86.8.820.
9. Sahashi, N.; Akiba, M.; Ishihara, M.; Abe, Y.; Morita, S. First report of the brown root rot disease caused by Phellinus noxius, its distribution and newly recorded host plants in the Amami Islands, southern Japan. *Forest Pathology* **2007**, *37*, 167-173, doi:https://doi.org/10.1111/j.1439-0329.2007.00491.x.

10. Oghenekaro, A.O.; Miettinen, O.; Omorusi, V.I.; Evueh, G.A.; Farid, M.A.; Gazis, R.; Asiegbu, F.O. Molecular phylogeny of Rigidoporus microporus isolates associated with white rot disease of rubber trees (Hevea brasiliensis). *Fungal Biology* **2014**, *118*, 495-506, doi:https://doi.org/10.1016/j.funbio.2014.04.001.
11. Chang, T.-T. Survival of Phellinus noxius in soil and in the roots of dead host plants. *Phytopathology* **1996**, *86*, 272-276.
12. Ding, S.; Hu, H.; Gu, J.-D. Diversity, Abundance, and Distribution of Wood-Decay Fungi in Major Parks of Hong Kong. *Forests* **2020**, *11*, 1030.
13. Hong, Y.; Tan, J.Y.; Xue, H.; Chow, M.L.; Ali, M.; Ng, A.; Leong, A.; Yeo, J.; Koh, S.M.; Tang, M.S.Y.; et al. A Metagenomic Survey of Wood Decay Fungi in the Urban Trees of Singapore. *Journal of Fungi* **2023**, *9*, 460.
14. Onsando, J.M. Wood rot disease of tea (Hypoxylon serpens): a review. *Tea* **1985**, *6*, 39-42.
15. Srivastava, D.S.; Kumar, R.; Singh, V. *Wood Decaying Fungi*; 2013.
16. Lundell, T.K.; Mäkelä, M.R.; de Vries, R.P.; Hildén, K.S. Chapter Eleven - Genomics, Lifestyles and Future Prospects of Wood-Decay and Litter-Decomposing Basidiomycota. In *Advances in Botanical Research*, Martin, F.M., Ed.; Academic Press: 2014; Volume 70, pp. 329-370.
17. Wu, F.; Zhou, L.-W.; Vlasák, J.; Dai, Y.-C. Global diversity and systematics of Hymenochaetaceae with poroid hymenophore. *Fungal Diversity* **2022**, *113*, 1-192, doi:10.1007/s13225-021-00496-4.
18. Murrill, W.A. Cuban Polypores and Agarics. *Mycologia* **1919**, *11*, 22-32, doi:10.2307/3753208.
19. Sakayaroj, J.; Preedanon, S.; Suetrong, S.; Klaysuban, A.; Jones, E.B.G.; Hattori, T. Molecular characterization of basidiomycetes associated with the decayed mangrove tree Xylocarpus granatum in Thailand. *Fungal Diversity* **2012**, *56*, 145 - 156.
20. Hattori, T.; Sakayaroj, J.; Jones, E.B.G.; Suetrong, S.; Preedanon, S.; Klaysuban, A. Three species of Fulvifomes (Basidiomycota, Hymenochaetales) associated with rots on mangrove tree Xylocarpus granatum in Thailand. *Mycoscience* **2014**, *55*, 344-354.
21. Saidi, N.B.; Al-Obaidi, J.R.; Fisol, A.F.b.C. Rigidoporus microporus and the white root rot disease of rubber. *Forest Pathology* **2023**, *53*, e12794, doi:https://doi.org/10.1111/efp.12794.
22. Wang, C.-G.; Vlasák, J.; Jin, C.; Si, J. Phylogeny and diversity of Rigidoporus (Hymenochaetales, Basidiomycota), including three new species from Asia. *Frontiers in Cellular and Infection Microbiology* **2023**, *13*, doi:10.3389/fcimb.2023.1216277.
23. Paul, H. Fungus diseases of tropical crops. *Commonwealth Mycological Institute, London* **1980**.
24. Go, W.Z.; Chin, K.L.; H'ng, P.S.; Wong, M.Y.; Luqman, C.A.; Surendran, A.; Tan, G.H.; Lee, C.L.; Khoo, P.S.; Kong, W.J. Virulence of Rigidoporus microporus isolates causing white root rot disease on rubber trees (Hevea brasiliensis) in Malaysia. *Plants* **2021**, *10*, 2123.
25. Farid, A.; Lee, S.; Maziah, Z.; Ehsan, S. Pathogenicity of Rigidoporus microporus and Phellinus noxius against four major plantation species in Peninsular Malaysia. *J. Trop. For. Sci.* **2009**, *21*.

26. Garfinkel, A.; Cannon, P.; Klopfenstein, N.; Stewart, J.; Kim, M.-S. *Identification of genetic groups within the invasive brown root rot pathogen, Pyrrhoderma noxium (formerly phellinus noxius)*; 2020.
27. Zhou, L.-W.; Ji, X.-H.; Vlasák, J.; Dai, Y.-C. Taxonomy and phylogeny of Pyrrhoderma: a redefinition, the segregation of Fulvoderma, gen. nov., and identifying four new species. *Mycologia* **2018**, *110*, 872-889, doi:10.1080/00275514.2018.1474326.
28. Sahashi, N.; Akiba, M.; Ishihara, M.; Ota, Y.; Kanzaki, N. Brown root rot of trees caused by Phellinus noxius in the Ryukyu Islands, subtropical areas of Japan. *Forest Pathology* **2012**, *42*, 353-361, doi:https://doi.org/10.1111/j.1439-0329.2012.00767.x.
29. Chung, C.L.; Huang, S.Y.; Huang, Y.C.; Tzean, S.S.; Ann, P.J.; Tsai, J.N.; Yang, C.C.; Lee, H.H.; Huang, T.W.; Huang, H.Y.; et al. The Genetic Structure of Phellinus noxius and Dissemination Pattern of Brown Root Rot Disease in Taiwan. *PLoS One* **2015**, *10*, e0139445, doi:10.1371/journal.pone.0139445.
30. Farid, A.; Lee, S.; Rosli, H.; Maziah, Z.; Muhammad, N. Incidence of teak basal root rot caused by Phellinus noxius in Malaysia. *Australasian Plant Pathology - AUSTRALAS PLANT PATHOL* **2005**, *34*, 277-278, doi:10.1071/AP05008.
31. Hodges, C.S.; Tenorio, J.A. Root disease of Delonix regia and associated tree species in the Mariana Islands caused by Phellinus noxius. *Plant Disease* **1984**, *68*, 334-336.
32. Chang, T.-T. Decline of some forest trees associated with brown root rot caused by Phellinus noxius. *Plant Pathology Bulletin* **1992**, *1*, 90-95.
33. Mardones, M.; Carranza-Velázquez, J.; Mata-Hidalgo, M.; Amador-Fernández, X.; Urbina, H. Taxonomy and phylogeny of the genus Ganoderma (Polyporales, Basidiomycota) in Costa Rica. *MycoKeys* **2023**, *100*, 5-47.
34. Karsten, P. Enumeratio Boletinearum et Polyporearum Fennicarum, systemate novo dispositarum. *Rev. Mycol.(Toulouse)* **1881**, *3*, 16-19.
35. Glen, M.; Bougher, N.L.; Francis, A.A.; Nigg, S.Q.; Lee, S.S.; Irianto, R.; Barry, K.M.; Beadle, C.L.; Mohammed, C.L. Ganoderma and Amauroderma species associated with root-rot disease of Acacia mangium plantation trees in Indonesia and Malaysia. *Australasian Plant Pathology* **2009**, *38*, 345-356.
36. Othman, N.Q.; Sulaiman, S.; Lee, Y.P.; Tan, J.S. Transcriptomic data of mature oil palm basal trunk tissue infected with Ganoderma boninense. *Data in brief* **2019**, *25*, 104288.
37. Ryvarden, L. Studies in neotropical polypores 2: a preliminary key to neotropical species of Ganoderma with a laccate pileus. *Mycologia* **2000**, *92*, 180-191.
38. Hapuarachchi, K.; Karunarathna, S.; Phengsintham, P.; Yang, H.; Kakumyan, P.; Hyde, K.; Wen, T. Ganodermataceae (Polyporales): Diversity in Greater Mekong Subregion countries (China, Laos, Myanmar, Thailand and Vietnam). **2019**.
39. Wong, L.; Bong, C.-F.J.; Idris, A. Ganoderma species associated with basal stem rot disease of oil palm. *American Journal of Applied Sciences* **2012**, *9*, 879-885.
40. Moncalvo, J.-M.; Wang, H.-H.; Hseu, R.-S. Phylogenetic relationships in Ganoderma inferred from the internal transcribed spacers and 25S ribosomal DNA sequences. *Mycologia* **1995**, *87*, 223-238.

41. Luangharn, T.; Karunarathna, S.C.; Dutta, A.K.; Paloi, S.; Promputtha, I.; Hyde, K.D.; Xu, J.; Mortimer, P.E. Ganoderma (Ganodermataceae, Basidiomycota) Species from the Greater Mekong Subregion. *J Fungi (Basel)* **2021**, *7*, doi:10.3390/jof7100819.
42. Yamashita, S.; Hirose, D. Phylogenetic analysis of Ganoderma australe complex in a Bornean tropical rainforest and implications for mechanism of coexistence of various phylogenetic types. *Fungal Ecology* **2016**, *24*, 1-6, doi:https://doi.org/10.1016/j.funeco.2016.04.006.
43. Goh, Y.K.; Tung, H.J.; Marzuki, N.F.; Hasim, I.; Wong, W.C.; Goh, K.J. FIRST REPORT OF GANODERMA AUSTRALE ON SCHIZOLOBIUM PARAHYBUM IN MALAYSIA. *Journal of Plant Pathology* **2014**, *96*, 435-435.
44. de Silva, N.I.; Phillips, A.J.L.; Liu, J.-K.; Lumyong, S.; Hyde, K.D. Phylogeny and morphology of Lasiodiplodia species associated with Magnolia forest plants. *Scientific Reports* **2019**, *9*, 14355, doi:10.1038/s41598-019-50804-x.
45. Abdollahzadeh, J.; Javadi, A.; Goltapeh, E.M.; Zare, R.; Phillips, A. Phylogeny and morphology of four new species of Lasiodiplodia from Iran. *Persoonia-Molecular Phylogeny and Evolution of Fungi* **2010**, *25*, 1-10.
46. Huda-Shakirah, A.R.; Mohamed Nor, N.M.I.; Zakaria, L.; Leong, Y.-H.; Mohd, M.H. Lasiodiplodia theobromae as a causal pathogen of leaf blight, stem canker, and pod rot of Theobroma cacao in Malaysia. *Scientific Reports* **2022**, *12*, 8966, doi:10.1038/s41598-022-13057-9.
47. Su, J.; Wang, T.; Tang, J.; Dong, X.; Dong, J.; Ji, P.; Zhang, L. Pathogenicity and identification of Lasiodiplodia theobromae causing Jatropha curcas stem canker in Yunnan, China. *Journal of General Plant Pathology* **2023**, *89*, 192-196, doi:10.1007/s10327-023-01118-4.
48. Gnanesh, B.N.; Arunakumar, G.S.; Tejaswi, A.; Supriya, M.; Manojkumar, H.B.; Devi, S.S. Characterization and Pathogenicity of Lasiodiplodia theobromae Causing Black Root Rot and Identification of Novel Sources of Resistance in Mulberry Collections. *Plant Pathol J* **2022**, *38*, 272-286, doi:10.5423/ppj.Oa.01.2022.0005.
49. Punithalingam, E. Botryodiplodia theobromae.[Descriptions of Fungi and Bacteria]. *Descriptions of Fungi and Bacteria* **1976**, Sheet 519.
50. Martinelli, F.; Scalenghe, R.; Davino, S.; Panno, S.; Scuderi, G.; Ruisi, P.; Villa, P.; Stroppiana, D.; Boschetti, M.; Goulart, L.; et al. Advanced methods of plant disease detection. A review. *Agronomy for Sustainable Development* **2014**, *35*, 1-25, doi:10.1007/s13593-014-0246-1.
51. Guglielmo, F.; Bergemann, S.E.; Gonthier, P.; Nicolotti, G.; Garbelotto, M. A multiplex PCR-based method for the detection and early identification of wood rotting fungi in standing trees. *Journal of Applied Microbiology* **2007**, *103*, 1490-1507, doi:https://doi.org/10.1111/j.1365-2672.2007.03378.x.
52. Holopainen, J.K.; Gershenzon, J. Multiple stress factors and the emission of plant VOCs. *Trends in Plant Science* **2010**, *15*, 176-184, doi:https://doi.org/10.1016/j.tplants.2010.01.006.

53. Wilson, A.D.; Lester, D.G.; Oberle, C.S. Development of Conductive Polymer Analysis for the Rapid Detection and Identification of Phytopathogenic Microbes. *Phytopathology*® **2004**, *94*, 419-431, doi:10.1094/phyto.2004.94.5.419.
54. Kigathi, R.N.; Weisser, W.W.; Reichelt, M.; Gershenzon, J.; Unsicker, S.B. Plant volatile emission depends on the species composition of the neighboring plant community. *BMC Plant Biology* **2019**, *19*, 58, doi:10.1186/s12870-018-1541-9.
55. Vivaldo, G.; Masi, E.; Taiti, C.; Caldarelli, G.; Mancuso, S. The network of plants volatile organic compounds. *Scientific Reports* **2017**, *7*, 11050, doi:10.1038/s41598-017-10975-x.
56. Guo, Y.; Jud, W.; Weikl, F.; Ghirardo, A.; Junker, R.; Polle, A.; Benz, J.P.; Pritsch, K.; Schnitzler, J.-P.; Rosenkranz, M. Volatile organic compound patterns predict fungal trophic mode and lifestyle. *Communications Biology* **2021**, *4*, doi:10.1038/s42003-021-02198-8.
57. Cellini, A.; Blasioli, S.; Biondi, E.; Bertaccini, A.; Braschi, I.; Spinelli, F. Potential Applications and Limitations of Electronic Nose Devices for Plant Disease Diagnosis. *Sensors* **2017**, *17*, 2596.
58. Falasconi, M.; Gobbi, E.; Pardo, M.; Della Torre, M.; Bresciani, A.; Sberveglieri, G. Detection of toxigenic strains of Fusarium verticillioides in corn by electronic olfactory system. *Sensors and Actuators B: Chemical* **2005**, *108*, 250-257, doi:https://doi.org/10.1016/j.snb.2004.09.046.
59. Baietto, M.; Pozzi, L.; Wilson, A.D.; Bassi, D. Evaluation of a portable MOS electronic nose to detect root rots in shade tree species. *Computers and Electronics in Agriculture* **2013**, *96*, 117-125, doi:https://doi.org/10.1016/j.compag.2013.05.002.
60. The Practical Guide to the Cyranose®320. **2013**.
61. The Cyranose® 320 eNose® User Manual. **2013**.
62. Wilson, A. Recent progress in the design and clinical development of electronic-nose technologies. *Nanobiosensors in Disease Diagnosis* **2016**, *5*, 15-27, doi:10.2147/NDD.S66278.
63. Karakaya, D.; Ulucan, O.; Turkan, M. Electronic Nose and Its Applications: A Survey. *International Journal of Automation and Computing* **2020**, *17*, 179-209, doi:10.1007/s11633-019-1212-9.
64. Dutta, R.; Hines, E.; Gardner, J.W.; Boilot, P. Bacteria classification using Cyranose 320 electronic nose. *Biomedical engineering online* **2002**, *1*, 4, doi:10.1186/1475-925X-1-4.
65. Ordukaya, E.; Karlik, B. Quality Control of Olive Oils Using Machine Learning and Electronic Nose. *Journal of Food Quality* **2017**, *2017*, 9272404, doi:10.1155/2017/9272404.
66. Markom, M.A.; Shakaff, A.Y.M.; Adom, A.H.; Ahmad, M.N.; Hidayat, W.; Abdullah, A.H.; Fikri, N.A. Intelligent electronic nose system for basal stem rot disease detection. *Computers and Electronics in Agriculture* **2009**, *66*, 140-146, doi:https://doi.org/10.1016/j.compag.2009.01.006.
67. Tan, J.Y. *Evaluation of the Electronic-nose and SPME GCMS for the diagnosis of three root rot fungi*; Nanyang Technological University: Singapore, 2021.

68. Gherghel, S.; Morgan, R.; Arrebola, F.; Romero-González, R.; Blackman, C.; Frenich, A.; Parkin, I. Development of a HS-SPME/GC-MS method for the analysis of volatile organic compounds from fabrics for forensic reconstruction applications. *Forensic Science International* **2018**, *290*, doi:10.1016/j.forsciint.2018.07.015.
69. Ouyang, G.; Pawliszyn, J. A critical review in calibration methods for solid-phase microextraction. *Analytica Chimica Acta* **2008**, *627*, 184-197, doi:https://doi.org/10.1016/j.aca.2008.08.015.
70. De Lacy Costello, B.P.J.; Evans, P.; Ewen, R.J.; Gunson, H.E.; Jones, P.R.H.; Ratcliffe, N.M.; Spencer-Phillips, P.T.N. Gas chromatography–mass spectrometry analyses of volatile organic compounds from potato tubers inoculated with Phytophthora infestans or Fusarium coeruleum. *Plant Pathology* **2001**, *50*, 489-496, doi:https://doi.org/10.1046/j.1365-3059.2001.00594.x.
71. Prithiviraj, B.; Vikram, A.; Kushalappa, A.C.; Yaylayan, V. Volatile Metabolite Profiling for the Discrimination of Onion Bulbs Infected by Erwinia carotovora ssp. carotovora, Fusariumoxysporum and Botrytis allii. *European Journal of Plant Pathology* **2004**, *110*, 371-377, doi:10.1023/B:EJPP.0000021058.81491.f8.
72. Loulier, J.; Lefort, F.; Stocki, M.; Asztemborska, M.; Szmigielski, R.; Siwek, K.; Grzywacz, T.; Hsiang, T.; Ślusarski, S.; Oszako, T.; et al. Detection of Fungi and Oomycetes by Volatiles Using E-Nose and SPME-GC/MS Platforms. *Molecules* **2020**, *25*, 5749.
73. Baietto, M.; Wilson, A.D.; Bassi, D.; Ferrini, F. Evaluation of Three Electronic Noses for Detecting Incipient Wood Decay. *Sensors* **2010**, *10*, 1062-1092.
74. Nord, F.F.; Vitucci, J.C. Enzyme Studies on the Mechanism of Wood Decay. *Nature* **1947**, *160*, 224-225, doi:10.1038/160224a0.
75. Sun, Y.; Li, Y.; Zhang, W.; Jiang, B.; Tao, S.-M.; Dai, H.-Y.; Xu, X.-T.; Sun, Y.-X.; Yang, L.; Zhang, Y.-J. The main component of the aphid alarm pheromone (E)-β-farnesene affects the growth and development of Spodoptera exigua by mediating juvenile hormone-related genes. *Frontiers in Plant Science* **2022**, *13*, doi:10.3389/fpls.2022.863626.
76. Zhao, G.; Maclean, A.L. A comparison of canonical discriminant analysis and principal component analysis for spectral transformation. *Photogrammetric Engineering and Remote Sensing* **2000**, *66*, 841-847.
77. Pryce, T.M.; Palladino, S.; Kay, I.D.; Coombs, G.W. Rapid identification of fungi by sequencing the ITS1 and ITS2 regions using an automated capillary electrophoresis system. *Med Mycol* **2003**, *41*, 369-381, doi:10.1080/13693780310001600435.
78. de Hoog, G.S.; Gerrits van den Ende, A.H. Molecular diagnostics of clinical strains of filamentous Basidiomycetes. *Mycoses* **1998**, *41*, 183-189, doi:10.1111/j.1439-0507.1998.tb00321.x.
79. Masclaux, F.; Guého, E.; de Hoog, G.S.; Christen, R. Phylogenetic relationships of human-pathogenic Cladosporium (Xylohypha) species inferred from partial LS rRNA sequences. *Journal of Medical and Veterinary Mycology* **1995**, *33*, 327-338, doi:10.1080/02681219580000651.

80. Izzah Hazirah Bte, J. *Monitoring of VOCs during In vitro pathogenesis of Rigidoporus microporus and Fulvifomes siamensis using SPME GC-MS and electronic nose*; Nanyang Technological University: 2023.
81. Tan, J.Y.; Zhang, Z.; Izzah, H.J.; Fong, Y.K.; Lee, D.; Mutwil, M.; Hong, Y. Volatile-Based Diagnosis for Pathogenic Wood-Rot Fungus Fulvifomes siamensis by Electronic Nose (E-Nose) and Solid-Phase Microextraction/Gas Chromatography/Mass Spectrometry. *Sensors (Basel)* **2023**, *23*, doi:10.3390/s23094538.
82. Manisalidis, I.; Stavropoulou, E.; Stavropoulos, A.; Bezirtzoglou, E. Environmental and Health Impacts of Air Pollution: A Review. *Frontiers in Public Health* **2020**, *8*, doi:10.3389/fpubh.2020.00014.
83. What Is Nitrogen Purging? – Procedure and Equipment Used. Available online: https://nigen.com/what-is-nitrogen-purging-procedure-services/#:~:text=Nitrogen%20purging%20is%20an%20industrial,system%20environment%20using%20nitrogen%20gas. (accessed on
84. Razo-Belmán, R.; Ángeles-López, Y.I.; García-Ortega, L.F.; León-Ramírez, C.G.; Ortiz-Castellanos, L.; Yu, H.; Martínez-Soto, D. Fungal volatile organic compounds: mechanisms involved in their sensing and dynamic communication with plants. *Frontiers in Plant Science* **2023**, *14*, doi:10.3389/fpls.2023.1257098.
85. Camarena‐Pozos, D.A.; Flores‐Núñez, V.M.; López, M.; Partida‐Martínez, L.P. Fungal volatiles emitted by members of the microbiome of desert plants are diverse and capable of promoting plant growth. *Environmental Microbiology* **2021**, *23*, 2215-2229.
86. Shahi, A.; Yu, H.; Mafu, S. Diterpene Biosynthesis in Rice Blast Fungus Magnaporthe. *Frontiers in Fungal Biology* **2022**, *3*, 869823.
87. Zhang, H.; Li, Y.; Mi, J.; Zhang, M.; Wang, Y.; Jiang, Z.; Hu, P. GC-MS Profiling of Volatile Components in Different Fermentation Products of Cordyceps Sinensis Mycelia. *Molecules* **2017**, *22*, 1800.
88. Wu, T.K.; Chen, C.H.; Pan, Y.R.; Hu, C.W.; Huang, F.M.; Liu, J.Y.; Lee, C.J. Cetrimonium Bromide Inhibits Cell Migration and Invasion of Human Hepatic SK-HEP-1 Cells Through Modulating the Canonical and Non-canonical TGF-β Signaling Pathways. *Anticancer Res* **2019**, *39*, 3621-3631, doi:10.21873/anticanres.13510.
89. Umesha, S.; Manukumar, H.M.; Raghava, S. A rapid method for isolation of genomic DNA from food-borne fungal pathogens. *3 Biotech* **2016**, *6*, 123, doi:10.1007/s13205-016-0436-4.
90. Harper, D.B.; Hamilton, J.T.; Kennedy, J.T.; McNally, K.J. Chloromethane, a Novel Methyl Donor for Biosynthesis of Esters and Anisoles in Phellinus pomaceus. *Appl Environ Microbiol* **1989**, *55*, 1981-1989, doi:10.1128/aem.55.8.1981-1989.1989.
91. Zelante, T.; Choera, T.; Beauvais, A.; Fallarino, F.; Paolicelli, G.; Pieraccini, G.; Pieroni, M.; Galosi, C.; Beato, C.; De Luca, A.; et al. Aspergillus fumigatus tryptophan metabolic route differently affects host immunity. *Cell Reports* **2021**, *34*, 108673, doi:https://doi.org/10.1016/j.celrep.2020.108673.

92. Gonçalves, S.M.; Duarte-Oliveira, C.; Campos, C.F.; Aimanianda, V.; ter Horst, R.; Leite, L.; Mercier, T.; Pereira, P.; Fernández-García, M.; Antunes, D.; et al. Phagosomal removal of fungal melanin reprograms macrophage metabolism to promote antifungal immunity. *Nature Communications* **2020**, *11*, 2282, doi:10.1038/s41467-020-16120-z.
93. Subko, K.; Kildgaard, S.; Vicente, F.; Reyes, F.; Genilloud, O.; Larsen, T.O. Bioactive Ascochlorin Analogues from the Marine-Derived Fungus Stilbella fimetaria. *Marine Drugs* **2021**, *19*, 46.
94. Grove, J.F. Volatile compounds from the mycelium of the mushroom Agaricus bisporus. *Phytochemistry* **1981**, *20*, 2021-2022, doi:https://doi.org/10.1016/0031-9422(81)84057-5.
95. Information, N.C.f.B. PubChem Compound Summary for CID 16221, Hexadecyldimethylamine. Available online: https://pubchem.ncbi.nlm.nih.gov/compound/Hexadecyldimethylamine (accessed on July 1).
96. Information, N.C.f.B. PubChem Compound Summary for CID 965, 9-Octadecenoic acid. Available online: https://pubchem.ncbi.nlm.nih.gov/compound/9-Octadecenoic-acid (accessed on July 1).
97. Zhang, Z. *Real time field application of the Cyranose 320 electronic nose for the diagnosis of Fulvifomes sp2012b root rot fungi.*; Nanyang Technological University: Singapore, 2022.
98. Lyr, H.; Werner, P. On the mechanism of action of the fungicide chloroneb. *Pesticide Biochemistry and Physiology* **1982**, *18*, 69-76, doi:https://doi.org/10.1016/0048-3575(82)90089-X.
99. Tillman, R.W.; Sisler, H.D. and Metabolism of Ustilago maydis. *Phytopathology* **1971**, *63*, 219-225.
100. Ishikawa, N.K.; Fukushi, Y.; Yamaji, K.; Tahara, S.; Takahashi, K. Antimicrobial Cuparene-Type Sesquiterpenes, Enokipodins C and D, from a Mycelial Culture of Flammulina velutipes. *Journal of Natural Products* **2001**, *64*, 932-934, doi:10.1021/np000593r.
101. Raafat, K. Identification of phytochemicals from North African plants for treating Alzheimer's diseases and of their molecular targets by in silico network pharmacology approach. *J Tradit Complement Med* **2021**, *11*, 268-278, doi:10.1016/j.jtcme.2020.08.002.
102. Sharma, A.; Bajpai, V.K.; Shukla, S. Sesquiterpenes and Cytotoxicity. In *Natural Products: Phytochemistry, Botany and Metabolism of Alkaloids, Phenolics and Terpenes*, Ramawat, K.G., Mérillon, J.-M., Eds.; Springer Berlin Heidelberg: Berlin, Heidelberg, 2013; pp. 3515-3550.
103. Dickschat, J.S.; Brock, N.L.; Citron, C.A.; Tudzynski, B. Biosynthesis of sesquiterpenes by the fungus Fusarium verticillioides. *Chembiochem* **2011**, *12*, 2088-2095, doi:10.1002/cbic.201100268.
104. Sá, S.; Chaul, L.T.; Alves, V.F.; Fiuza, T.S.; Tresvenzol, L.M.F.; Vaz, B.G.; Ferri, P.H.; Borges, L.L.; Paula, J.R. Phytochemistry and antimicrobial activity of

Campomanesia adamantium. *Revista Brasileira de Farmacognosia* **2018**, *28*, 303-311, doi:https://doi.org/10.1016/j.bjp.2018.02.008.
105. Dickschat, J.S. Fungal volatiles - a survey from edible mushrooms to moulds. *Nat Prod Rep* **2017**, *34*, 310-328, doi:10.1039/c7np00003k.
106. Blasioli, S.; Biondi, E.; Braschi, I.; Mazzucchi, U.; Bazzi, C.; Gessa, C.E. Electronic nose as an innovative tool for the diagnosis of grapevine crown gall. *Analytica chimica acta* **2010**, *672 1-2*, 20-24.

Appendixes

Appendix A

A

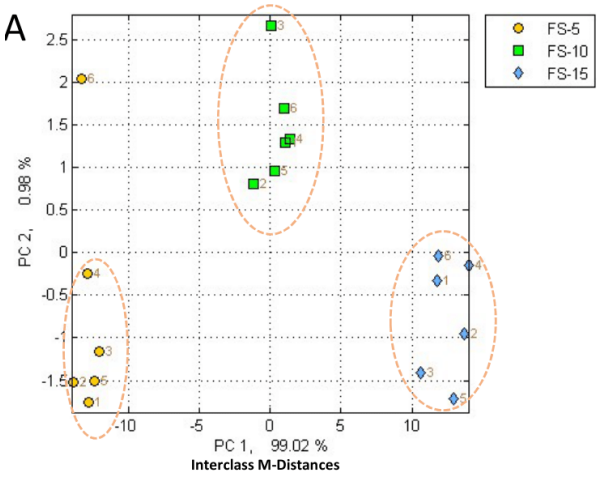

Interclass M-Distances

	FS-5	FS-10	FS-15
FS-5		13.518	25.366
FS-10			12.223

B

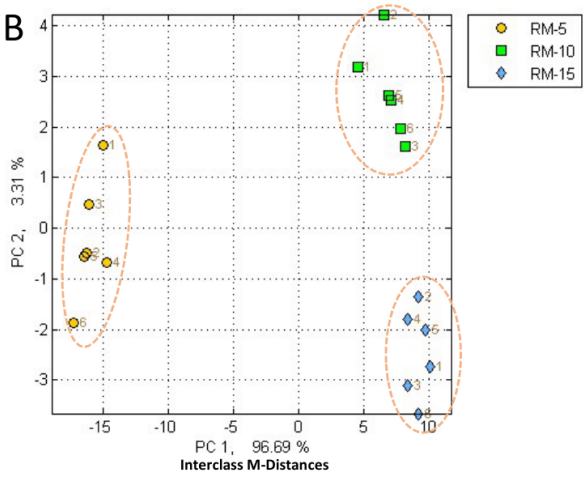

Interclass M-Distances

	RM-5	RM-10	RM-15
RM-5		23.049	25.262
RM-10			5.627

C

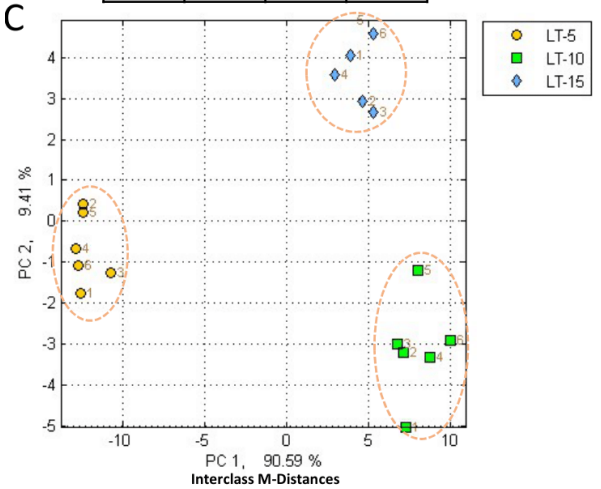

Interclass M-Distances

	LT-5	LT-10	LT-15
LT-5		20.481	17.251
LT-10			7.806

D

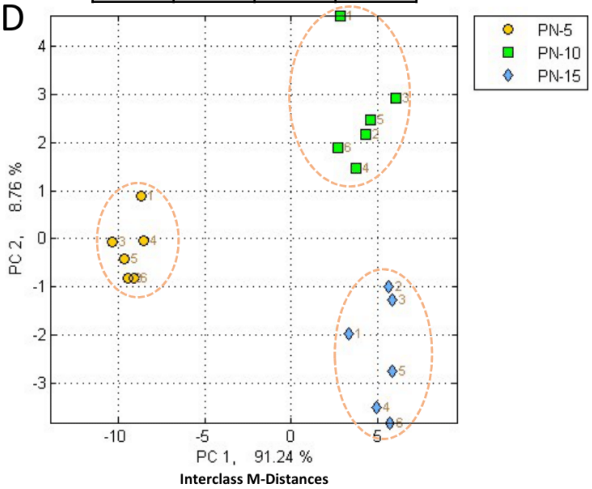

Interclass M-Distances

	PN-5	PN-10	PN-15
PN-5		13.641	14.686
PN-10			5.122

Appendix A continued

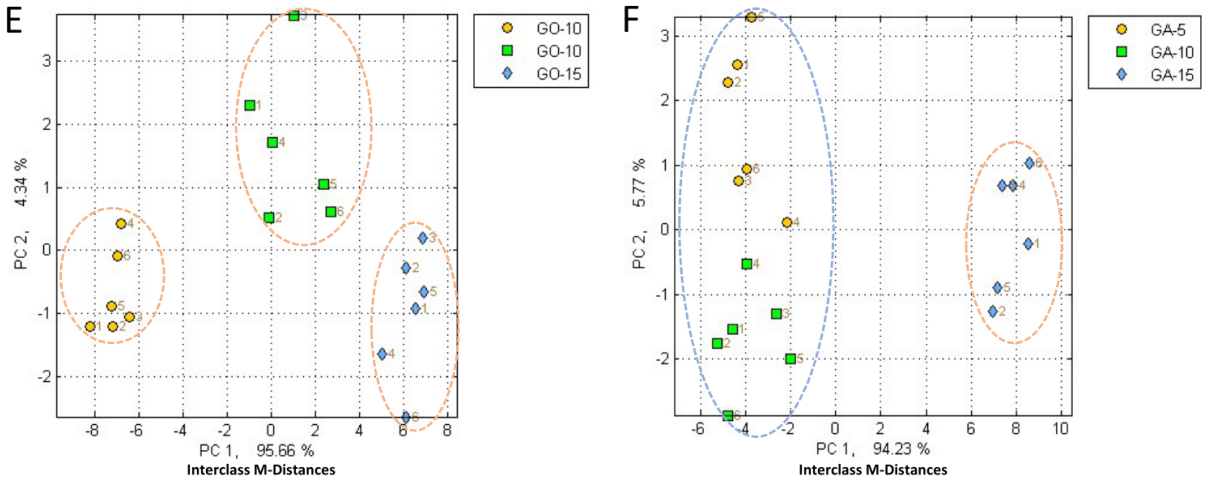

	GO-5	GO-10	GO-15
GO-5		8.336	13.436
GO-10			6.033

	GA-5	GA-10	GA-15
GA-5		3.318	11.744
GA-10			11.721

Appendix A: Scatter plots with Canonical Discriminant Analysis (CDA) and calculated Interclass M-Distances (MDist) on e-nose volatile readings of varying fungi mycelia cut plug numbers. A: Plots with five, ten, and fifteen fungal mycelia cut plugs for *F. siamensis* (FS-5, FS-10, FS-15); **B**: Plots with five, ten, and fifteen fungal mycelia cut plugs for *R. microporus* (RM-5, RM-10, RM-15); **C**: Plots with five, ten, and fifteen fungal mycelia cut plugs for *L. theobromae* (LT-5, LT-10, LT-15); **D**: Plots with five, ten, and fifteen fungal mycelia cut plugs for *P. noxium* (PN-5, PN-10, PN-15); **E**: Plots with five, ten, and fifteen fungal mycelia cut plugs for *G. orbiforme* (GO-5, GO-10, GO-15); **F**: Plots with five, ten, and fifteen fungal mycelia cut plugs for *G. australe* (GA-5, GA-10, GA-15). Samples inside an orange dashed-line ellipse indicate that the MDist is greater than 5.000 and thus form a distinctive cluster. Samples inside a blue dashed-line ellipse indicate a cluster of two samples with MDist less than 5.000, which is also indicated in blue in the pairwise comparison Interclass M-Distances table. Figure A and B adapted from Tan et. al [81].

Appendix B

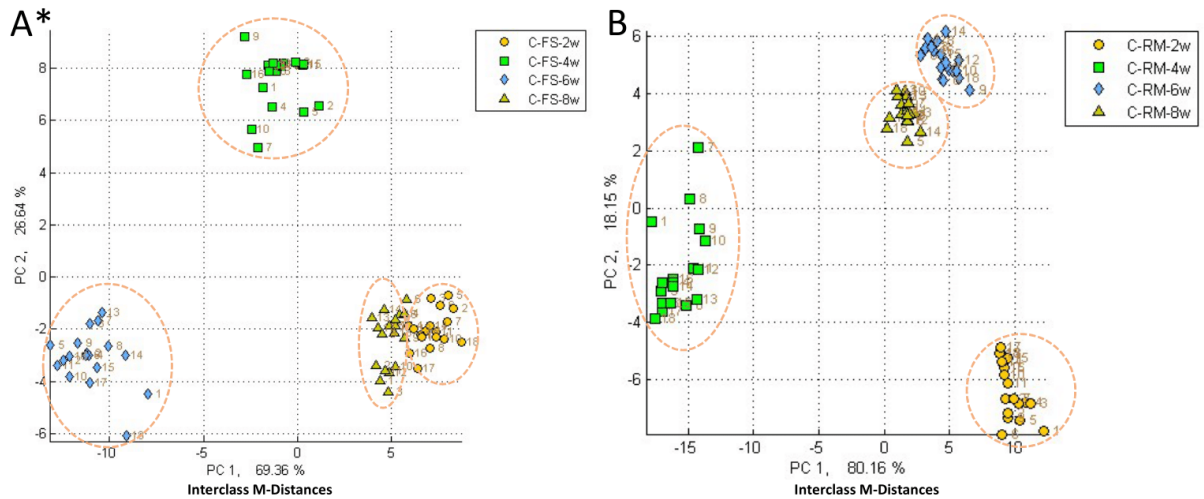

	C-FS-2w	C-FS-4w	C-FS-6w	A-FS-8w
C-FS-2w		12.796	18.278	5.252
C-FS-4w			14.536	11.824
C-FS-6w				16.181

	C-RM-2w	C-RM-4w	C-RM-6w	C-RM-8w
C-RM-2w		25.801	12.720	12.883
C-RM-4w			21.561	18.311
C-RM-6w				5.182

Appendix B continued

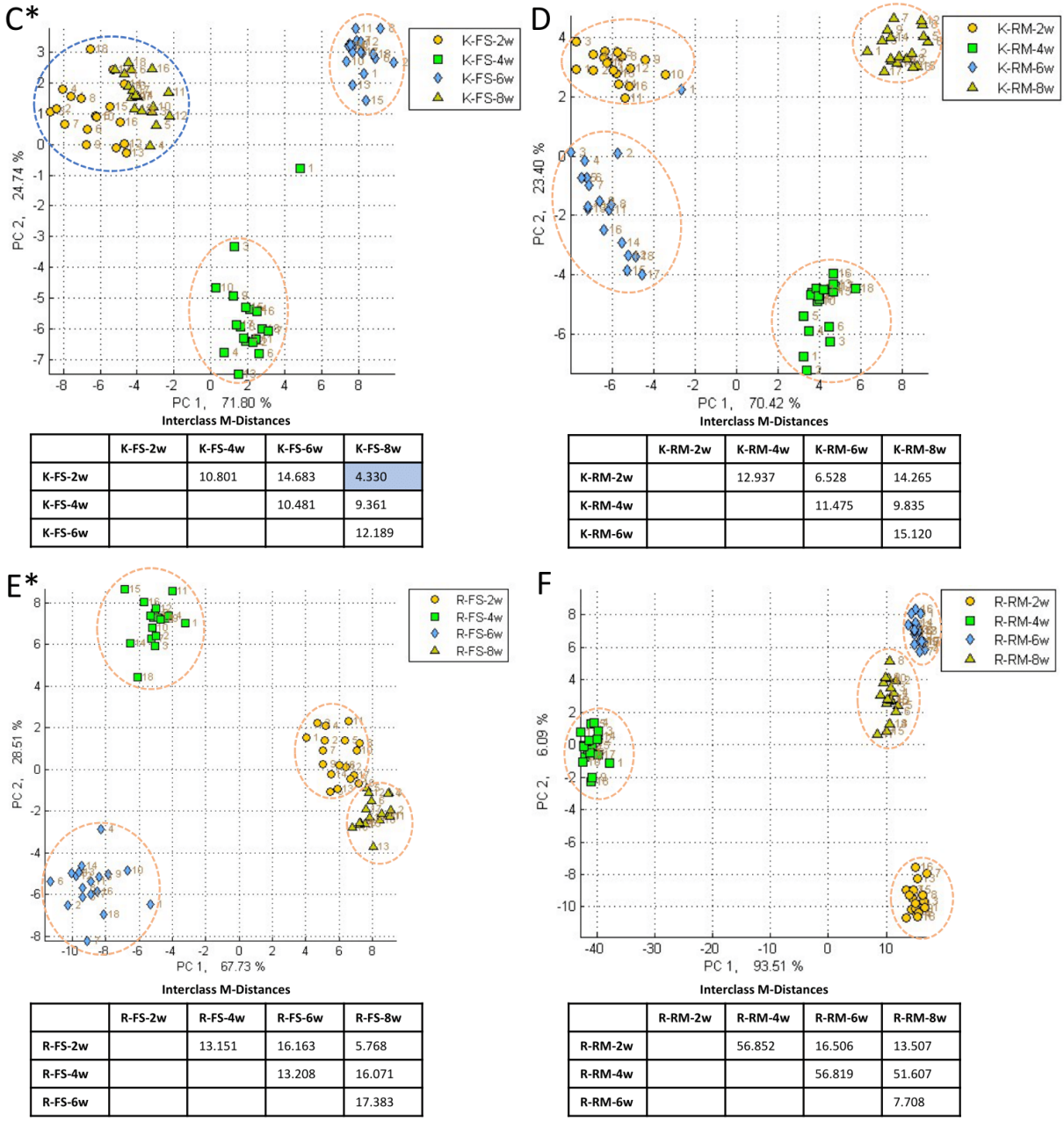

	K-FS-2w	K-FS-4w	K-FS-6w	K-FS-8w
K-FS-2w		10.801	14.683	4.330
K-FS-4w			10.481	9.361
K-FS-6w				12.189

	K-RM-2w	K-RM-4w	K-RM-6w	K-RM-8w
K-RM-2w		12.937	6.528	14.265
K-RM-4w			11.475	9.835
K-RM-6w				15.120

	R-FS-2w	R-FS-4w	R-FS-6w	R-FS-8w
R-FS-2w		13.151	16.163	5.768
R-FS-4w			13.208	16.071
R-FS-6w				17.383

	R-RM-2w	R-RM-4w	R-RM-6w	R-RM-8w
R-RM-2w		56.852	16.506	13.507
R-RM-4w			56.819	51.607
R-RM-6w				7.708

Appendix B: Scatter plots with Canonical Discriminant Analysis (CDA) and calculated Interclass M-Distances (MDist) on e-nose volatile readings of Casuarina, Khaya, and Rain tree wood blocks after varying incubation periods with wood rot fungi based. A: Wood blocks of Casuarina tree with two weeks (C-FS-2w), four weeks (C-FS-4w), six weeks (C-FS-6w), eight weeks (C-FS-8w) of fungal treatment with *F. siamensis*; **B**: Wood blocks of Casuarina tree with two weeks (C-RM-2w), four weeks (C-RM-4w), six weeks (C-RM-6w), eight weeks (C-RM-8w) of fungal treatment with *R. microporus*; **C**: Wood blocks of Khaya tree with two weeks (K-FS-2w), four weeks (K-FS-4w), six weeks (K-FS-6w), eight weeks (K-FS-8w) of fungal treatment with *F. siamensis*; **D**: Wood blocks of Khaya tree with two weeks (K-RM-2w), four weeks (K-RM-4w), six weeks (K-RM-6w), eight weeks (K-RM-8w) of fungal treatment with *R. microporus*; **E**: Wood blocks of Rain tree with two weeks (R-FS-2w), four weeks (R-FS-4w), six weeks (R-FS-6w), eight weeks (R-FS-8w) of fungal treatment with *F. siamensis*; **F**: Wood blocks of Rain tree with two weeks (R-RM-2w), four weeks (R-RM-4w), six weeks (R-RM-6w), eight weeks (R-RM-8w) of fungal treatment with *R. microporus*. Samples inside an orange dashed-line ellipse indicate that the MDist is greater than 5.000 and thus form a distinctive cluster. Samples inside a blue dashed-line ellipse indicates a cluster of two samples with MDist less than 5.000, which is also indicated in blue in the pairwise comparison table. * indicates that the number of PCs used for the canonical graph was 15 instead of 10 (default).